MEASUREMENT OF $N_2 X^1\Sigma_g^+$ ROTATIONAL AND VIBRATIONAL TEMPERATURES OVER A 300° K TO 1100° K RANGE USING A HIGH-ENERGY ELECTRON BEAM

A Thesis

Presented to

The Faculty of the Department of Physics

The College of William and Mary in Virginia

In Partial Fulfillment

Of the Requirements for the Degree of

Master of Arts

by

William Winslow Hunter, Jr.

August 1965

OF ΔN2 ΔX(1 ΔSIGMA g + PLUS)

MEASUREMENT OF $N_2 X^1\Sigma_g^+$ ROTATIONAL AND VIBRATIONAL TEMPERATURES OVER A 300° K TO 1100° K RANGE USING A HIGH-ENERGY ELECTRON BEAM

A Thesis

Presented to

The Faculty of the Department of Physics

The College of William and Mary in Virginia

In Partial Fulfillment

Of the Requirements for the Degree of

Master of Arts

By

William Winslow Hunter, Jr.

August 1965

ACKNOWLEDGMENTS

The author wishes to thank Dr. G. S. Ofelt for his suggestions and guidance. The encouragement received from Dr. J. D. Lawrence, Jr. is appreciated. Thanks are expressed to Mr. M. L. Emory and Mr. J. C. Hoppe for their assistance in preparation of the many figures and tables. Finally, the National Aeronautics and Space Administration and its graduate study program must be recognized for making this work possible.

TABLE OF CONTENTS

LIST OF FIGURES

FIGURE PAGE

FIGURE PAGE

LIST OF TABLES

ABSTRACT

The purpose of this work was to determine the validity of the theory (ref. 1) for measuring rotational and vibrational temperatures of $N_2 X^1\Sigma_g^+$ from the spectral characteristics of the gas fluorescence caused by inelastic collisions between gas molecules and high energy electrons (25-28 Kev). The initial investigator conducted experiments for two gas temperatures, approximately 300° K and 373° K. These experiments were conducted in a flowing low density nitrogen gas.

The experiments reported here were performed in a static gas, in thermal equilibrium. The test gas was air and the data were obtained from the nitrogen constituent. Rotational temperature measurements were conducted over a 300° K to 1100° K range. Both the 0-0 and 0-1 bands of the first negative system of nitrogen were used for the measurements.

The experiments were performed in a unique test chamber which was designed for this work. The test chamber permitted control of the test gas pressure and temperature over a continuous range of 1.3 to 133.3 N/m^2 and approximately 300° K to 1100° K, respectively. Data were obtained with the aid of a 0.5 meter Fastie-Ebert scanning spectrometer.

The results of the experiments indicated that the rotational temperature may be measured with at least ±8 percent accuracy over a 300° K to 1100° K range. Vibrational temperature measurement results were within an estimated accuracy of ±18 percent.

MEASUREMENT OF $N_2 X^1\Sigma_g^+$ ROTATIONAL AND VIBRATIONAL TEMPERATURES OVER A 300° K TO 1100° K RANGE USING A HIGH-ENERGY ELECTRON BEAM

INTRODUCTION

Thermal equilibrium conditions of a molecular system may be determined by measuring and comparing the molecular translational, rotational, and vibrational temperatures. Rotational and vibrational temperature may be determined through the application of the well-known spectral emission intensity equation to spectroscopic observations of a thermally excited gas.

The rotational and vibrational temperature of a low-temperature gas, which radiates very weakly, is of physical interest also. It is known that high-energy electrons may be used to cause gas fluorescence. The question then arises: Can the radiation, as a result of high-energy electron inelastic collisions with gas molecules, be used for determining rotational and vibrational temperature? The answer to this question is contained in the validity of the theory for determining the relative number density population of the rotational and vibrational energy levels of the excited electronic state.

The initial investigator (ref. 1), who formulated the theory for this application, experimentally investigated the validity of the theory for the rotational temperature measurements for two test temperatures, approximately 300° K and 373° K. These experiments were conducted in a flowing nitrogen gas and the data were obtained only from the 0-0 band of the nitrogen first negative system.

The purpose of the experiments reported here was to enable an investigation of the validity of the theory for rotational temperature measurements over a range from 300° K to 1100° K. Rotational temperature measurements were made from data obtained from the 0-0 band as well as the 0-1 band of the nitrogen first negative system. These experiments were conducted in a static test gas, in thermal equilibrium. This procedure avoided any corrections that might be required for a dynamic gas condition.

Vibrational temperature experiments were also conducted at 300° K and 400° K. These data were taken under the same test conditions as existed for the rotational measurements.

The temperature measurements that were obtained from a pure N_2 test gas were found to be the same, within experimental error, as those obtained with air as the test gas. The data presented here were obtained from the experiments conducted in air.

The procedure for this investigation was to pass high-energy electrons through a static test gas at a known temperature. The gas was contained in a test chamber which could be maintained at a desired temperature and pressure. With the test gas under controlled conditions, measurements of the rotational and vibrational temperature were performed and compared with a reference temperature. This comparison provided the basis for determining the applicability of the theory over a range of temperatures.

The first portion of this paper outlines and develops the theory similar to that as presented in reference 1. This is followed by a description of the experimental system and test procedure. Finally, the experimental data and results are presented.

CHAPTER I

THEORY

Introduction

The test gas used in this investigation was air and the primary sources of visible and near ultraviolet radiation were the first negative and second positive systems of nitrogen. The first negative system is a source of intense and resolvable spectrum and because of the abundance of available information concerning this system and similar work done by others (refs. 1 and 2) this system was selected for investigation. The excitation and emission path for the first negative system is illustrated by an energy level diagram (fig. 1). A high-energy electron, designated as a primary electron, is emitted by a source and has an inelastic collision with a ground state nitrogen molecule, $N_2X^1\Sigma_g^+$. The molecule is excited to the excited ionized state, $N_2^+B^2\Sigma_u^+$, from which it spontaneously radiates and drops into the ground ionized energy state, $N_2^+X^2\Sigma_g^+$. The intensity and spectral distribution of the spontaneous emitted radiation reflects the vibrational and rotational characteristics of the molecules that were in the $N_2X^1\Sigma_g^+$ state.

Rotational and vibrational temperatures may be obtained from an application of the intensity of emission equation

$$I_{em}^{nm} = N_n h c \nu_{nm} A_{nm} \qquad (1)$$

where $hc\nu_{nm}$ is the energy of the emitted radiation as a result of the transition between states n and m, ν_{nm} is the wave number of the emitted radiation, A_{nm} is the transition probability of emission, and N_n is the number density population of the initial level of transition. An inspection of equation (1) shows that all terms are constants or dependent only on the particular transition involved except N_n. Application of equation (1) requires the determination of the population and its distribution in the initial level, $N_2^+B^2\Sigma_u^+$. The following section will present arguments for determining the population source of $N_2^+B^2\Sigma_u^+$ and following this will be a discussion of the excitation-transition process and the development of an intensity of emission equation which relates the observed emission to the electron beam excitation process for obtaining rotational and vibrational temperature.

Primary $N_2^+B^2\Sigma_u^+$ Population Source

Determination of the population of $N_2^+B^2\Sigma_u^+$ state of nitrogen requires consideration of sources. The sources as a result of primary electron inelastic collisions are:

1. $N_2X^1\Sigma_g^+$
2. Excited states of N_2
3. $N_2^+X^2\Sigma_g^+$

Comparison of the cross sections for excitation to discrete excited states of N_2 and for ionization of N_2, hereafter designated as excitation and ionization cross sections, respectively, provides a means for estimating the population contributions to N_2^+ from excited N_2 states relative to the contribution from $N_2X^1\Sigma_g^+$ state. The excitation cross section may be calculated from (ref. 3)

$$\sigma = \sum_{n} 8\pi \left(\frac{e}{h\nu}\right)^2 \left|(d_x)_{on}\right|^2 \ln q \qquad (2)$$

where the sum is over the discrete states of neutral nitrogen and (d_x) is the x-component of the dipole moment. The momentum transfer, q, includes the scattering angle which is limited in the Born approximation to (ref. 3)

$$\theta \ll v_o/v \qquad (3)$$

v is the velocity of the primary electron (1×10^{10} cm/sec for this work) and v_o is of the order of magnitude of the velocity of an atomic electron. The upper limit of the scattering angle is about 1^o.

The ionization cross section may be determined from theoretical curves for energy loss of electrons per unit path length as a function of electron potential (ref. 4), knowing that 33 to 35 ev are required to form an ion pair (ref. 4) and the molecular number density of the test gas.

The resultant ratio of the ionization cross section to the excitation cross section is at least 10 to 1 and is probably 100 to 1 for primary electrons with a velocity of 1×10^{10} cm/sec. This observation is substantiated by the experimental results of this and other works (ref. 1). The number of excited N_2 molecules excited to $N_2^+B^2\Sigma_u^+$ through a second inelastic collision will be insignificant in comparison with the number of $N_2X^1\Sigma_g^+$ molecules excited directly to $N_2^+B^2\Sigma_u^+$. Also, the number of ionized molecules in the $N_2^+X^2\Sigma_g^+$ state that are excited to

$N_2^+B^2\Sigma_u^+$ will be small since the excitation cross section for ionized molecules is expected to be of the same order of magnitude as that for nonionized molecules. But, the number of molecules excited to $N_2^+X^2\Sigma_g^+$ from $N_2X^1\Sigma_g^+$ may be about equal to the number excited to $N_2^+B^2\Sigma_u^+$ since the ionization cross sections would be approximately equal. If the cross sections are approximately equal and since $N_2^+B^2\Sigma_u^+$ and other excited states of N_2^+ may spontaneously radiate and drop into the $N_2^+X^2\Sigma_g^+$ state, it is possible that the number of molecules excited to $N_2^+B^2\Sigma_u^+$ from $N_2^+X^2\Sigma_g^+$ would be significant. However, the experimental results of this work and others (refs. 1 and 2) indicate that this is not the case. Therefore, the population source of $N_2^+B^2\Sigma_u^+$, as a result of inelastic collisions with primary electrons, is primarily $N_2X^1\Sigma_g^+$.

Secondary electrons and their possible effect on the population of $N_2^+B^2\Sigma_u^+$ may be determined qualitatively by considering two energy ranges, above and below ionization threshold. Secondaries which have energies in excess of the ionization threshold, approximately equal to 16 ev, do not present any significant problems unless the excitation by these relatively slow electrons is different from that of the primary electrons. Previous investigators have not observed such a difference (refs. 1 and 2). Secondaries which have energies less than 16 ev would have to have inelastic collisions with excited molecules in order to ionize. Therefore, it is believed that the number of ions resulting from inelastic collisions with secondaries of 16 ev or less is small compared with the ions resulting from primary electrons and secondaries

Cascading from various ionized states of N_2^+ to $N_2^+B^2\Sigma_u^+$ is another possible population source. An inspection of the potential curves and energy levels of the various excited ionized states which have been observed (ref. 6) shows that most transitions to $N_2^+B^2\Sigma_u^+$ are parity forbidden or that the resultant overlap integral would be very small.

It may be concluded from the preceding discussion that the primary population source for $N_2^+B^2\Sigma_u^+$ is $N_2X^1\Sigma_g^+$ and is a result of inelastic collisions of molecules in the $N_2X^1\Sigma_g^+$ energy state with primary electrons and secondaries with energies of 16 ev or larger.

Excitation-Transition Process

In order to determine the population of the vibrational and rotational energy states of $N_2^+B^2\Sigma_u^+$, the excitation-transition process must be evaluated. The excitation process is a function of the excitation conditions including excitation cross section and electron current and potential. The excitation function may be represented by a term C_e which is a constant for a particular electron transition.

In order to calculate the transition probabilities for the excitation process, it is necessary to represent the initial and final molecular states with an appropriate wave function. The relative mass of the atomic nuclei and electrons was considered in selecting the appropriate wave function. Because the mass difference is very large, the velocity of the nuclei is small compared to the velocity of the orbital electrons. Therefore, the motion of the orbital electrons is taken to be about a fixed nuclei configuration. With the preceding

consideration, the Born-Oppenheimer approximation for the molecular wave function is made.

The wave function for diatomic molecules in the Born-Oppenheimer approximation is

$$\psi_{evJ\Lambda M} = \psi_e(\bar{r}_i,\bar{r}_N)\,\frac{1}{r_N}\,\psi_v(r_N)\psi_{J\Lambda M}(\theta,\chi,\varphi) \tag{4}$$

where ψ_e is the electronic wave function with the ith electronic coordinate $\bar{r}_i$ referenced to the molecular axis, ψ_v is the vibrational wave function with nuclei separation r_N, and $\psi_{J\Lambda M}$ the rotational wave function which is a function of the Euler angles (θ, χ, φ). The Euler angles relate the molecular coordinate system to the coordinate system of the fixed point of observation. Also, it is assumed that the interaction of the primary electron with the orbital electrons can be described by a coulombic potential. Therefore, the following matrix element of this interaction may be used to describe the excitation.

$$\left(e_{P'},e_S,B^2\Sigma_u^+v'J'\Lambda'M'\left|\sum_i \frac{e^2}{r_{1i}}\right|e_{P''}X^1\Sigma_g^+v''J''\Lambda''M''\right) \tag{5}$$

In the above expression, the initial and final wave functions of the primary electrons are represented by $e_{P''}$ and $e_{P'}$, e_S, the secondary electron, $X^1\Sigma_g^+$ and $B^2\Sigma_u^+$ represent the initial and final electronic wave functions, v" and v' the vibrational states, and J"Λ"M" and J'Λ'M' the rotational states. Of course, $\sum_i \frac{e^2}{r_{1i}}$ is the coulombic interaction term where the quantity r_{1i} is the distance between the high-energy primary electron and the ith orbital electron.

It should be noted that in the notation to be used later, prime superscripts refer to $N_2^+B^2\Sigma_u^+$ states, double prime superscripts with

a one (1) subscript refers to $N_2X^1\Sigma_g^+$ states and double prime superscripts with a two (2) subscript refers to $N_2^+X^2\Sigma_g^+$ states.

Since the particular transition of interest results in the removal of one orbital electron and for simplicity $\sum_i \frac{1}{r_{1i}}$ will be replaced with $\frac{1}{r_{12}}$ where the removed electron is labeled with a subscript 2. The removed orbital electron is a $\sigma_u 2s$ electron from $N_2X^1\Sigma_g^+$ to form $N_2^+B^2\Sigma_u^+$, therefore, the electronic state may be expressed as $X^1\Sigma_g^+ \equiv \left[B^2\Sigma_u^+\sigma_u 2s\right]$ (ref. 7). Equation (5) is now rewritten as

$$\left(e_p, e_s, B^2\Sigma_u^+ v'K'\Lambda'M' \left| \frac{e^2}{r_{12}} \right| e_p'' \left[B^2\Sigma_u^+\sigma_u 2s\right] v''K''\Lambda''M''\right) \tag{6}$$

Note that K has been used in place of J; this may be done from consideration of the applicable coupling scheme which is Hund's case (b) (ref. 7), and by suppressing the spin angular momentum.

In order to evaluate this matrix element for high-energy primary electrons, a plane wave approximation is made for the primary electron wave functions and the integration over the primary electron coordinates is performed. This integration gives (ref. 3)

$$\int e_p'(\bar{r}_1)\left(\frac{1}{r_{12}}\right)e_p''(\bar{r}_1)d\bar{r}_1 = \frac{4\pi}{q^2} e^{i\bar{q}\cdot\bar{r}_2} \tag{7}$$

where $\bar{q}$ is the momentum transfer and $\bar{r}_2$ is the position vector of the interacting orbit electron. At this point a series expansion of $e^{i\bar{q}\cdot\bar{r}_2}$ is made

$$e^{i\bar{q}\cdot\bar{r}_2} = 1 + i\bar{q}\cdot\bar{r}_2 - \frac{1}{2}(\bar{q}\cdot\bar{r}_2)^2 + \ldots \tag{8}$$

To a first-order approximation the first two terms of the above expansion are retained. But the contribution from the first term in equation (8) is

zero because of the orthogonality of the initial and final states of the molecule. Therefore, equation (6) is given by

$$\frac{4\pi}{q^2} e^2 (e_S, B^2\Sigma_u^+ v'K'\Lambda'M' \left| i\bar{q} \cdot \bar{r}_2 \right| \left[B^2\Sigma_u^+ \sigma_u 2s \right] v''K''\Lambda''M'') \qquad (9)$$

In order to evaluate equation (9) further, the vector $\bar{r}_2$ is transformed to the coordinates of the molecular axis through the dyadic $\bar{\bar{D}}(\theta, X, \varphi)$ which relates the molecular coordinate axis to the fixed coordinate system of the point of observation. Therefore, equation (9) is rewritten

$$\frac{i4\pi e^2 \bar{q}}{q^2} \cdot (K'\Lambda'M' \left| D(\theta,X,\varphi) \right| K''\Lambda''M'') \cdot (e_S, B^2\Sigma_u^+ v' \left| \bar{r}_2' \right| \left[B^2\Sigma_u^+ \sigma_u 2s \right] v'') \qquad (10)$$

The absolute value squared of the term $\frac{i4\pi e^2 \bar{q}}{q^2}$ is contained in the excitation function, C_e, and will be suppressed in the following equations.

Equation (10) provides the rotational quantum number selection rules of $\Delta K = \pm 1$ for $\Lambda'' = \Lambda' = 0$ transitions. In addition, when equation (10) is squared and the summation of the quantum numbers M'' and M' is performed the results give the band and line strength terms.

The square of the second matrix element is defined as the band strength, or the vibrational transition probability, and is designated $P_{v'v''}$. Band strength $P_{v'v''}$ may be approximated by assuming a mean value of the internuclear separation. Then the second matrix element of equation (10) may be written

$$P_{v'v''} = \left|(e_S, B^2\Sigma_u^+|\bar{r}_2'|[B^2\Sigma_u^+\sigma_u 2s])\right|^2 \left|(v'/v'')\right|^2 \tag{11}$$

The overlap integral of the vibrational wave functions squared $\left|(v'/v'')\right|^2$ is the well-known Franck-Condon factor, $q_{v'v''}$. Generally, equation (11) is then expressed as

$$P_{v'v''} = \left|R_{ij}^e\right|^2 q_{v'v''} \tag{12}$$

In order to take into account the variation of internuclear separation, a method of $\bar{r}$ centroids (ref. 15) is used where $\bar{r}$ is the expectation value of the internuclear separation, r_N, as determined by the vibrational wave functions. Now, the band strength is given by

$$P_{v'v''} = \left|R_{ij}^e(\bar{r}_N)\right|^2 q_{v'v''} \tag{13}$$

The rotational line strength is given by the first matrix element of equation (10) squared, summed over M'' and M'

$$\sum_{M'M''} \left|(K'\Lambda'M'|\bar{D}|K''\Lambda''M'')\right|^2 \tag{14}$$

This term is the well-known Hönl-London factor $S_{K''\Lambda''}^{K'\Lambda'}$ which is well tabulated (ref. 7). For the transition of interest, the relative rotational line strength may be obtained through the ratio of the line strength to the sum of the line strengths, that is,

$$P_R^a = \frac{S_{K''}^{K'}}{\sum_{K'} S_{K''}^{K'}} \tag{15}$$

This equation is the relative line strength for excitation-transition which is indicated by the superscript a. The relative line strength for emission is the same except the summation is over K" and is designated P_R^e.

The preceding work of this section has been based on a plane wave approximation for the high-energy incident primary electron. It is necessary to consider low-energy secondary electrons since these may contribute significantly to the number of ionized nitrogen molecules. Several observations may be made without making a detailed analysis of the excitation-transition process. It should be noted that for electronic states of the homonuclear nitrogen molecule, $X^1\Sigma_g^+$ and $B^2\Sigma_u^+$ rotational levels have symmetric and antisymmetric states under nuclear exchange. The symmetry properties of $X^1\Sigma_g^+$ and $B^2\Sigma_u^+$ are the opposite with respect to even and odd rotational quantum numbers. And, only transitions between rotational energy levels with the same symmetry are allowed. Therefore, the same selection rules with respect to ΔK for high-energy electrons apply to low-energy electrons. The only difficulty would be if the first-order approximation is not sufficiently accurate such that $\Delta K = \pm 3$ transitions would contribute appreciably in order to describe secondary electron-induced transitions. If this were so it would affect the resultant rotational temperature measurements. However, this had not been observed in previous investigations (ref. 1). Also, it is assumed that the factorization of equations (12) and (13) is still valid.

Vibrational Temperature, T_v

The intensity of spontaneously emitted radiation as a result of transitions between two vibrational energy states is given by

$$I_{v',v_2''} = N_{v'} hc\nu_{v',v_2''} A_{v',v_2''} \tag{16}$$

where $A_{v',v_2''}$ is the transition probability of spontaneous emission for transitions between initial vibrational level, v', and a terminal vibrational level, v_2'', and $\nu_{v',v_2''}$ is the wave number of the resultant radiation of the transition. Vibrational temperature may be determined by measuring the intensity of a vibrational band (ref. 7), provided the number density population, $N_{v'}$, has a Boltzmann distribution. However, for this work, this is not the situation. The number density population $N_{v'}$ and its distribution is a function of the source level population, distribution, and the excitation-transition process.

For this work it has been shown that $N_2 X^1\Sigma_g^+$ is the primary source of molecules which are excited to $N_2^+ B^2\Sigma_u^+$ as a result of inelastic electron collisions. Therefore, $N_{v'}$ and the resultant intensity of spontaneous emission is dependent on the distribution and the number density population of the vibrational energy states, $N_{v_1''}$, of $N_2 X^1\Sigma_g^+$. The steady-state relation between $N_{v'}$ and $N_{v_1''}$ as a result of inelastic electron N_2 collision is given by

$$N_{v'} = \frac{C_e}{R} \sum_{v_1''} N_{v_1''} P_{v',v_1''} \tag{17}$$

where the product $C_e \sum_{v_1''} P_{v',v_1''}$ describes excitation and transition process between v_1'' and v'. C_e is the excitation function and $P_{v',v_1''}$

is the vibrational band strength described in the preceding section, and R is the depopulation rate. The term C_e/R will be designated C_e' henceforth. If it is assumed that the $N_2X^1\Sigma_g^+$ vibrational energy states are in thermal equilibrium, then the number of molecules in a given $N_{v_1''}$ vibrational state is given by a Boltzmann distribution

$$N_{v_1''} = \frac{N_o}{Q_v} e^{-E_{v_1''}/kT_v} \tag{18}$$

where $Q_v = \sum_{v_1''} e^{-E_{v_1''}/kT_v}$ is the "state sum" or partition function, $E_{v_1''} = e^{-G_o(v_1'')hc/kT_v}$ the characteristic energy of the v_1'' level, $G_o(v_1'')$ the vibrational term, N_o the steady-state population of $N_2X^1\Sigma_g^+$, and T_v the vibrational temperature. Therefore, with the substitution of equation (18) into equation (17), the dependence of $N_{v'}$ on the T_v of $N_2X^1\Sigma_g^+$ is established, and the relation between vibrational temperature of $N_2X^1\Sigma_g^+$ and the intensity of spontaneous emitted radiation, equation (16), can be determined.

It is not necessary to make absolute intensity measurements since T_v may be determined through ratio of intensities of two vibrational bands. The resultant equation, as derived from equations (16), (17), and (18), is

$$\frac{I_{v_o'v_2''}}{I_{v_1'v_2''}} = \frac{\sum_{v_1''} e^{-E_{v_1''}/kT_v} P_{v_o'v_1''} A_{v_o'v_2''} \nu_{v_o'v_2''}}{\sum_{v_1''} e^{-E_{v_1''}/kT_v} P_{v_1'v_1''} A_{v_1'v_2''} \nu_{v_1'v_2''}} \tag{19}$$

Note that C'_e, N_o, and Q_v canceled in the above ratio since these terms are independent of a particular $v' - v''_1$ transition. Therefore, with equation (19), the variation of the intensity ratio as a function of T_v may be calculated. As an example, the calculation for the intensity ratio for the 0-1 and 1-2 bands is shown in figure 2. The transition probabilities used for this example were obtained from references 8 and 9.

Rotational Temperature, T_R

It is shown in references 7, 10, and 11 that a rotational temperature may be determined by measuring the relative intensities of the rotational fine structure spectrum. However these measurements are based on the assumption that the initial level of the transition is in thermal equilibrium. But, as mentioned previously, this is not the case for this investigation. The initial level rotational number density, $N_{K'}$ of $N_2^+B^2\Sigma_u^+$, is a function of the excitation-transition process, depopulation rate, and number density, $N_{K''_1}$ of $N_2X^1\Sigma_g^+$. If it is assumed that rotational states of a v''_1 are in thermal equilibrium, then $N_{K''_1}$ is given by (ref. 7)

$$N_{K''_1} = \frac{N_{v''_1}}{Q_r}(2K''_1 + 1)e^{-E_{K''_1}/kT_R} \tag{20}$$

where $Q_r = \sum_{K''} (2K'' + 1)e^{-E_{K''_1}/kT_R}$ is the rotational partition function, $E_{K''_1} = e^{-F(K''_1)hc/kT_R}$ the characteristic energy of a rotational state, $F(K''_1)$ the rotational term, and T_R the rotational temperature. Again, notice that a relation to a temperature has been established through the

Boltzmann factor based on the explicit assumption that thermal equilibrium exists in the ground electronic state of the neutral species of N_2.

In order to interpret this temperature dependence in the resulting intensity of radiation, the selection rules for transitions between various rotational energy states are applied. The applicable selection rule given in the excitation-transistion section is $\Delta K = \pm 1$. Therefore, the resultant total angular momentum change is $\Delta J = \pm 1 \pm 1/2$ where the $\pm 1/2$, that is, spin angular momentum, reflects the removal of an orbital electron.

The effects of electron spin increase with the rotational quantum number and results in line splitting of approximately 0.4 cm^{-1} for $K_2'' = 23$, which is the practical limit of observation. The ratio of line spacing to spin splitting for $K_2'' = 23$ is 50 to 1. Therefore, spin splitting in comparison with rotational line separation is negligible. Because the ratio of line spacing to spin splitting is large and the spin splitting is experimentally unresolved in this work, an effective summation over spin components is performed. The transition may then be formally described by $^1\Sigma - {}^1\Sigma$ and the associated selection rule is $\Delta K = \pm 1$.

The $\Delta K = \pm 1$ selection rule predicts the formation of a P-branch ($\Delta K = -1$) and R-branch ($\Delta K = +1$) in the rotational fine structure of a vibrational band in excitation as well as emission.

With the formation of the P- and R-branches, the steady-state population of $N_2^+ B^2\Sigma_u^+$ is given by*

*The following derivation is similar to that of reference 1 by E. P. Muntz.

$$N_{K'} = C'_e \sum_{v''_1} \left\{ \left[N''_{K''+1} P^a_{RR} + N''_{K''-1} P^a_{RP} \right] \cdot P_{v'v''_1} \right\} \tag{21}$$

where P^a_{RR} and P^a_{RP} are the relative rotational line strengths of absorption, previously described, for the P- and R-branches. Writing P^a_{RR} and P^a_{RP} in terms of K' (ref. 7)

$$P^a_{RR} = \frac{K'}{2K' - 1} \tag{22}$$

$$P^a_{RP} = \frac{K' + 1}{2K' + 3} \tag{23}$$

Now, by using equations (22) and (23) and expressing equation (20) in K' terms through the selection rule $\Delta K = \pm 1$

$$N''_{K''+1} P^a_{RR} = \frac{N_{v''_1}}{Q_r} K' e^{-E_{K'-1}/kT_R} \tag{24}$$

$$N''_{K''-1} P^a_{RP} = \frac{N_{v''_1}}{Q_r} (K' + 1) e^{-E_{K'+1}/kT_T} \tag{25}$$

With the above expressions, equation (21) may be written as

$$N_{K'} = C'_e \sum_{v''_1} \left[\frac{N_{v''_1} P_{v'v''_1} (A)}{Q_r} \right] \tag{26}$$

where

$$(A) = K' e^{-E_{K'-1}/kT_R} + (K' + 1) e^{-E_{K'+1}/kT_R} \tag{27}$$

Term (A) is defined for ease of manipulation.

With the determination of $N_{K'}$, the intensity of emitted radiation may be calculated as a function of the rotational temperature, T_R. Before the calculation may be accomplished, it is necessary to set up an expression for the emission transition probability, $A_{v'K',v_2''K_2''}$.

$$A_{v'K',v_2''K_2''} = X\nu^3 P_{v'v_2''} P_R^e \tag{28}$$

where X is a constant, ν is the wave number of the transition, and P_R^e is the relative rotational transition probability for emission. P_R^e for emission is given by (ref. 7)

$$P_{RR}^e = \frac{K'}{2K' + 1} \qquad \text{(R-branch)} \tag{29}$$

$$P_{RP}^e = \frac{K' + 1}{2K' + 1} \qquad \text{(P-branch)} \tag{30}$$

In emission only the R-branch is suitable for practical use since it can be easily resolved.

Therefore, the intensity of emission for a particular R-branch transition is given by

$$I_{K'K_2''} = XC_e'\nu^4 \sum_{v_1''} \left[\frac{\frac{N_o}{Q_v} e^{-E_{v_1''}/kT_v} P_{v'v_1''}(A)}{Q_r} \right] \left(\frac{K'}{2K' + 1} \right) P_{v'v_2''} \tag{31}$$

This equation is simplified by noting that the product

$$XC_e'P_{v'v_2''}N_o/Q_v \tag{32}$$

is a constant, Z, for a particular $v' - v_2''$ transition. Also, the equation may be put in conventional form (ref. 7) by noting that $2K' = K' + K_2'' + 1$ for R-branch transitions. Therefore,

$$\frac{I_{K'K_2''}}{K' + K_2'' + 1} = \frac{Z\nu^4}{2K' + 1} \sum_{v_1''} \left[\frac{P_{v'v_1''} e^{-E_{v_1''}/kT_v} (A)}{Q_r} \right] \tag{33}$$

For the case of $T_v \lesssim 800^\circ$ K, 99 percent of the total population is in the $v_1'' = 0$ level. Equation (33) may now be written

$$\frac{I_{K'K_2''}/I_o}{K' + K_2'' + 1} = Z'\nu^4 [G] e^{-B_o K'(K'+1)hc/kT_R} \tag{34}$$

where

$$Z' = \frac{ZP_{v'o}\, e^{-E_o/kT_v}}{Q_r I_o} \tag{35}$$

$$[G] = \frac{K' e^{2B_o K' hc/kT_R} + (K' + 1) e^{-2B_o(K'+1)hc/kT_R}}{2K' + 1} \tag{36}$$

Note that a reference intensity I_o has been included to permit the measurements of relative intensities. The new term $[G]$ involves T_R and requires a solution of equation (34) through a process of iteration.

For the case of T_v of 800° K $\lesssim T_v \leq 1100^\circ$ K, only a small error is introduced by assuming that equation (34) applies to this case. The error is small since less than 5 percent of the total population of $N_2 X^1\Sigma_g^+$ at $T_v = 1100^\circ$ K occupies the upper vibrational states. The error introduced in the calculated T_R by this approximation is less than 2 percent and the measurement accuracy in the 800° K to 1100° K region is no better than 5 percent, therefore, equation (34) will be applied to the range of 300° K to 1100° K.

For ease of application, equation (34) is put in the following form:

$$\frac{B_o hc}{kT_R} K'(K' + 1) + Z'' = -2.3 \log_{10}\left[\frac{I_{K'K_2''}/I_o}{(K' + K_2'' + 1)\left\{[G](\nu/\nu_o)^4\right\}}\right] \qquad (37)$$

where ν_o is a reference wave number used to normalize ν. Following reference 1, ν_o value is chosen for $K' - K_2'' = 3\text{-}2$ transition. Also, Z'' is just the $\log_{10}$ of Z', which is a constant.

CHAPTER II

EXPERIMENTAL SYSTEM

The purpose of this section is to describe the apparatus and major characteristics of the experimental system. The experimental system (fig. 3 and, for example, fig. 13) may be divided into three subsystems: test gas temperature and vacuum control, electron beam, and optical and electronic detector system.

Test Gas Temperature and Vacuum Control System

The test gas temperature and vacuum control system (figs. 4 and 5) was designed to provide flexibility in temperature and vacuum test conditions. Temperature and pressure operating ranges are approximately 300° K to 1100° K and 133.3 to 6.7×10^{-3} N/m^2 (1 torr $\approx$ 133.3 newton/meter^2).

The major component of the system is the test chamber which consists of three concentric cylinders. The outer cylinder is a stainless steel water-cooled jacket and is fitted with vacuum-tight water-cooled top and bottom covers. Each cover is fitted with large flanges, attached to extensions, for mounting test hardware. Three 3-inch optical grade quartz windows are located in the outer cylinder wall. The next concentric cylinder consists of a helically wound nickel ribbon heating element (fig. 6) and is attached to ceramic supporting rods. Electrical connections are made to

copper electrodes which extend through the outer cylinder. The inner cylinder is an 8-inch-diameter 15-inch-long stainless steel electrostatic shield (fig. 7) and is grounded together with the outer cylinder to prevent charge buildup on the walls. Also, the inner cylinder provides a more uniform heating surface for the test gas than would be provided by the ribbon heating element. The inner cylinder is equipped with end covers which have openings for passage of the electron beam. Three 1-1/2 inch diameter openings are provided in the cylinder wall and are located in line with the viewing windows of the outer cylinder.

Rectified heater current is supplied from a 440 Vac 3-phase system. Temperature control is provided by coarse and fine rheostats. Temperature is regulated within $\pm 10^{\circ}$ K of the preset value by an on-off automatic pyrometer. A maximum operating temperature of 1100° K was obtained for a heating element voltage and current of 35 Vdc and 50 amperes.

A 35 psi water cooling system is provided as a heat sink for the outer chamber wall and covers, as well as cooling the diffusion pump. An interlock system prevents operation of the heating system and diffusion pump unless proper cooling flow is established.

A 5 CFM mechanical pump, 750 liter/sec diffusion pump, cold trap and necessary isolating valves comprise the vacuum pumping system. A variable leak valve, with air dryer, in combination with the mechanical pump was used to maintain the test chamber at the desired pressure. Vacuum conditions of the test chamber are monitored by two types of detectors. The pressure range from 133.3 to 1.3×10^{-1} N/m^2 is monitored

by a thermocouple-type vacuum gage, and from 1.3×10^{-1} to 6.7×10^{-3} N/m^2 is covered by an ionization-type vacuum gage.

Test Chamber Temperature Survey

A temperature survey of the inner cylinder wall was conducted to establish wall temperatures for various reference temperatures. Twelve thermocouples were attached, with bolts, to the inner cylinder wall and monitored with a 24-channel recorder. The thermocouples and recorder were calibrated with standard temperature sources.

The thermocouples were divided into three groups of four. One group was located midway between the ends of the cylinder, the other two groups were located 2-1/2 inches from the ends. The four thermocouples in each group were equally spaced about the cylinder circumference. One thermocouple of the center group was located at the same point as the pyrometer sensing thermocouple which was selected as the reference temperature point.

The resultant inner chamber temperature versus indicated pyrometer temperature curve is shown in figure 8. An extrapolation of the data from 780° K to 1100° K was necessary because of the limited range of the recorder.

A second survey was conducted in conjunction with the first survey with an electron beam current of 1000 μA passing through the test gas with the test chamber at approximately 300° K. The temperature of the reference point was 7° K higher than without the beam. The lowest group of thermocouples was 14° K higher and the upper group was 5° K higher. A similar test was conducted with the test chamber reference

point at 600° K. But, at this higher temperature, no detectable inner wall temperature difference between the test without the beam and with the beam were noted.

Next, a temperature survey was conducted to determine the inner container bottom plate heating caused by scattered primary and secondary electrons. Ten thermocouples were attached to the under side of the plate. The temperature of the point monitored by the inner thermocouple No. 4 (fig. 9) varied from 288° K for no beam, to 383° K for a 1450 μA beam. For the same beam current range, the outer thermocouple No. 1 varied from 288° K to only 338° K. The variations of temperature with current were, however, difficult to establish because the center of the beam shifted slightly with changes in beam current.

These results indicated that heating was present due to scattered primary and secondary electrons impinging on the bottom plate of the inner cylinder. This created a small temperature gradient through the length and across the radius of the test chamber. The temperature gradient through the length decreased with an increase in wall temperature and the data indicated some variations could be expected radially.

Electron Beam System

The purpose of the electron beam system is to supply high-energy electrons, 25 to 28 Kev. The electron beam system is illustrated in a block diagram (fig. 10) and the design and construction details are covered in reference 12.

The electron gun (figs. 11 and 12) is insulated from the test chamber. Since the chamber is at ground potential and serves as the

beam collector, the current measured by the micro-microammeter is the beam current.

The electron gun was operated at pressures of 1.3×10^{-2} N/m^2 or less. In order to maintain the gun pressure lower than the test chamber pressure, a 2-1/2 cm long plug with a 1-mil hole is placed in the end of the drift tube (fig. 11). This arrangement causes a pressure gradient across the length of the opening. With an increase of chamber pressure to approximately 53.2 N/m^2, the gun pressure rises above the upper operating limit.

Optical and Electronic Detector System

The purpose of the optical and electronic detector system is to analyze the test gas fluorescence. A block diagram (fig. 13) illustrates the system.

The major component of this system is the 0.5 meter Fastie-Ebert mount scanning spectrometer. This instrument has 16.0 Å/mm dispersion in the first order and a 0.2 Å resolution. A photomultiplier tube which has a quartz window and S-13 spectral response characteristic is mounted at the exit slit. The high-voltage power supply for the photomultiplier has a stability of 0.005 percent per hour.

The micro-microammeter is a vacuum tube electrometer with an amplifier used to drive a strip chart recorder which has been modified to have a floating zero. The response of the available recorder was 1 second full scale which is slower than the 0.5 second of the amplifier. Based on the relative slow response of the recording system, a 5 Å/min scanning spectrometer speed was required.

The relative spectral response of the spectrometer, photomultiplier, and lens, as a system, was determined. This calibration was accomplished by using a standard tungsten lamp source whose spectral characteristic was known. The correction factor for intensity ratio of the 0-1/1-2 bands was 0.97.

CHAPTER III

EXPERIMENTAL DATA

Data Acquisition

The relative rotational line and vibrational band intensities are required to determine the rotational and vibrational temperatures of the test gas. A detectable radiation level was obtained by operating the electron beam system to deliver 900 μA, or greater, and maintaining the test chamber at a pressure of approximately 26.6 N/m^2 at 300° K.

The 0-0 and 0-1 bands of N_2^+ were selected for the rotational temperature measurements since these are the strongest bands in the temperature range of this work. Spectral surveys of these bands were performed with a 25-micron spectrometer slit width so that the instrument width would be greater than the line width which allows line intensity values to be determined directly from the recorded peak values. Also, 25-micron slit width is sufficiently narrow to obtain the necessary resolution.

Surveys were made at 100° K intervals over the test chamber range, 300° K to 1100° K. A recording of a band used for a rotational temperature measurement is shown in figure 14.

The 0-1 and 1-2 bands of N_2^+ were selected for the vibrational temperature measurements since there is no overlapping by second positive systems of N_2 and no strong overlapping by other first negative bands of N_2^+ at low temperatures. The relative band intensities for this

work were obtained by measuring peak values of the P-branch envelope. It was necessary to select a spectrometer slit width of 250 microns to obtain sufficient spectral width to cover the P-branch between the band origin and band head. For vibrational temperatures equal to or less than 400° K, the major portion of the P-branch intensity is contained between the band origin and band head and that portion which lies beyond the band origin may be neglected with no more than 2 percent error.

Data Reduction

Once the recorded traces, similar to those shown in figures 14 and 15, have been obtained, rotational and vibrational temperatures may be determined. The procedure for the rotational temperature measurement is to measure the peak value of a rotational line and enter this value into equation (37) for $I_{K'K''_2}$. It is necessary at this point to make an estimate of the rotational temperature by noting the rotational line at which maximum intensity is recorded. With the aid of this estimate, a value for $\left\{[G](\nu/\nu_o)^4\right\}$ is determined from tables 1 or 2. This procedure is repeated for each rotational line. The next step is to plot each point, for strong lines, on a graph (e.g., fig. 16), then by least squares fit determine the best straight line. From the slope of the curve, a rotational temperature may be determined. If this value does not agree with the estimated value, the process is repeated with another temperature estimate and this process is repeated until the estimated and calculated temperatures fall within the smallest temperature division of the table of $\left\{[G](\nu/\nu_o)^4\right\}$ values. The entire procedure is repeated for the weak line system of the band.

For rotational temperatures of 400° K or less, vibrational temperature is determined by the ratio of the peak values of the P-branch envelopes of 0-1 and 1-2 bands. This measured ratio is then corrected for the spectral calibration factor. The corrected value is applied to the curve of figure 2 to give a vibrational temperature.

For rotational temperatures above 400° K, the peak of P-branch may not be used satisfactorily because the upper rotational levels become more heavily populated, with the corresponding lines falling outside of the spectral width viewed by the spectrometer. Also, there is strong overlapping of the R-branch of the 0-1 band on the P-branch of the 1-2 band. The procedure at these temperatures is to measure the total area under each band trace. The 1-2 band area must be corrected for the overlap by 0-1 band.

CHAPTER IV

RESULTS

Rotational Temperature Measurement Results

Experimental rotational temperature measurements and associated plots are shown in figures 16 through 33. A weighted mean temperature and standard deviation for each N_2^+ band, 0-0 and 0-1, for each test temperature is given in tables 3 and 4. The weighted mean temperature is determined from the measured temperatures given by the strong and weak line systems of a band. Finally, a plot of percent difference between the weighted mean temperature and reference temperature is presented in figure 34.

Figure 34 shows that the largest error between the measured and reference temperatures is no greater than ±8 percent. Therefore, this work demonstrated that reasonably accurate rotational temperature measurements between 300° K and 1100° K can be made by observing gas fluorescence that is a result of inelastic collisions between electrons and gas molecules. In addition, the measurements show that the relative number density population of $N_2^+ B^2\Sigma_u^+$ could be determined with sufficient accuracy to permit good rotational temperature measurements.

Figures 16 through 33 illustrate good straight line fit of the data points. This good straight line fit indicates that the steady-state population distribution within the N_2 ground electronic state, $N_2 X^1\Sigma_g^+$, was Boltzmann, and the Boltzmann distribution was not significantly disturbed by the high-energy electrons.

An examination of figures 16 through 33 shows that the number of points which fall below the curves increases with temperature. The deviation of these points is the result of the overlapping of the P-branch on the R-branch. The amount of overlapping increases with an increase in population of the upper rotational energy levels which increases with temperature. When the intensity of a P-branch rotational line is approximately 1 percent of the intensity of an adjacent R-branch rotational line, then the resultant measured line intensity is significantly affected. Therefore, using the 1 percent criteria, all affected R-branch lines were not included in the temperature measurement.

Vibrational Temperature Measurement Results

Vibrational temperature measurements were conducted only for low temperatures, 300° K and 400° K. The experiments, for vibrational temperatures, were restricted to these low temperatures because there is a strong overlap of the 0-1 band on the 1-2 band at the higher temperatures. Measurements could have been made for higher temperatures but would have required an estimated correction for the overlap. This correction would increase with temperature and would be difficult to determine accurately. Therefore, it was felt that the low temperature measurements were sufficient to show the adequacy of the theory and transition probabilities used. Also, the relative number population of the vibrational energy levels, $v' = 0$ and $v' = 1$, could be determined. The results of these measurements are shown in figure 2. The resultant measurements were accurate within ±18 percent.

Errors

The errors which affected the preceding results may be divided into random and systematic errors. The most important error which affected the accuracy of this work appears to be systematic. This systematic error is apparent in figure 34. A definite plus to minus change of percent difference between weighted mean temperature and reference temperature is noted as the reference temperature is increased for both N_2^+ bands. This is probably due to a difference between the true gas temperature and the reference temperature as a result of electron beam heating of the bottom plate. The assumption that there is probably a difference between the reference temperature and true gas temperature is based on several observations. First, it should be noted that to determine the true gas temperature, at the point of observation, is very difficult. It is difficult, even in a static environment, because the accuracy of measurements by any type of probe is affected by gas density, conduction, convection, radiation, and even the probe itself. These effects which must be corrected for are extremely difficult to determine. Also, the determination of the true gas temperature with any physical sensing probe, at the point of test observations, is even more difficult when the electron beam is passing through the chamber.

Even with all the above difficulties, the magnitude of the effect of the electron beam heating on the bottom plate may be judged from the observations given in the Test Chamber Temperature Survey section. It was pointed out that an increase in the inner cylinder wall temperature was noted with the beam on when the reference temperature was approximately

300° K. This increase in wall temperature was only 7° K at the reference point. Therefore, it appears that the heating at the point of observation would not be too large. It was also noted that at 600° K no noticeable change in wall temperature with the beam on was noted. Therefore, the effects of the electron beam heating on the gas temperature are small. Note that it was in the 600° K to 700° K region of figure 34 that the best agreement was obtained.

Coupling the above observations with the observations of references 1 and 2, which showed that measured gas rotational temperature was independent of beam current and potential, it appears reasonable to assume that a systematic error exists. The conclusion is that this systematic error is due to the difference between reference temperature and true gas temperature.

The random errors which affected the rotational temperature measurements are chart reading errors with a maximum of ±3 percent and errors due to signal noise, approximately ±2 percent. In most all cases the mean square deviation of all data points was less than the error assigned to these causes. Also, the good agreement of the data to a straight line shows that random errors were small.

The major uncertainties affecting the vibrational temperature measurements are contained in the transition probabilities, ±10 percent, accuracy of the recorded data, ±3 percent, and the calibration of the optical-electronic system, ±5 percent. An overall uncertainty of ±18 percent was assigned for the vibrational measurements.

CHAPTER V

CONCLUSIONS

Rotational Temperature Measurements

Experiments that were performed showed that the theory presented here for determining the rotational temperature of the ground electronic state of nitrogen from the relative intensities of the rotational structure of nitrogen's first negative system was reasonably accurate for the 300° K to 1100° K temperature range. The results of the experiments indicated a minimum accuracy agreement with theory of ±8 percent. In addition, it was found that rotational temperature measurements of $N_2 X^1\Sigma_g^+$ could be performed equally well with the 0-0 and 0-1 bands of N_2^+.

Vibrational Temperature Measurements

The experimental measurements of the vibrational temperature of the ground electronic state of nitrogen were within the estimated measurement accuracy of ±18 percent. The experimental results show that the theory, for the determination of the vibrational temperature of $N_2 X^1\Sigma_g^+$ in air from the relative band intensities of N_2^+, was at least as accurate as the transitional probabilities used in this work. It was also shown that with the proper spectrometer slit width the vibrational temperatures may be determined from the relative peak values of the P-branches of the 0-1 and 1-2 bands of N_2^+ for rotational temperatures equal to or less than 400° K.

Discussion

Improvement in the accuracy of the measurements could be realized through a more precise temperature measurement of the test gas. It is possible that this could be obtained through modification of the test chamber which would be directed toward obtaining a more uniform test gas temperature throughout the interior. A more uniform temperature could be obtained by heating the top and bottom of the inner cylinder. Another possibility might be to create a low-velocity air flow in the test chamber.

It also would be of interest to conduct experiments for the measurement of rotational and vibrational temperatures for test gas temperature equal to or less than 300° K. These experiments would yield useful information on the validity of the theory in the low-temperature region where the population is concentrated in the low rotational energy levels. Also, at these temperatures the magnitude of the overlapping of various adjacent bands of N_2^+ would decrease significantly and could be neglected with an error of less than 1 percent which would permit the determination of various vibrational transition probabilities more accurately.

SYMBOLS

(A)	defined by equation (27)
A_{nm}	transition probability for emission between states n and m
$A_{v'v_2''}$	transition probability for emission between vibrational energy states v' and v_2''
$A_{v'K',v_2''K_2''}$	transition probability for emission between rotational energy states K' and K_2''
B_o	rotational constant related to the vibrational level $V_1'' = 0$
$B_{v_1''}$	rotational constant related to the vibrational level v_1''
$B^2\Sigma_u^+$	represents the electronic wave function for $N_2^+B^2\Sigma_u^+$
C_e	excitation function which describes the electron-molecular excitation process
C_e'	ratio of the excitation function to depopulation rate of $N_2^+B^2\Sigma_u^+$ state
c	speed of light
$(d_x)_{on}$	dipole moment, x component
$E_{K_1''}$	characteristic energy of K_1'' rotational energy level
$E_{v_1''}$	characteristic energy of v_1'' vibrational energy level
e	electron charge
$e_{p'}$, $e_{p''}$	primary electron
e_s	secondary electron
$F(K_1'')$	rotational term (ref. 7)

$[G]$	defined by equation (36)
$G_o(V_1'')$	vibrational term (ref. 7)
h	Planck's constant
I_{em}^{nm}	intensity of emission for transitions between n and m states
$I_{K'K_2''}$	intensity of emission for transitions between K' and K'' rotational energy levels
I_o	reference intensity of emission
$I_{v'v_2''}$	intensity of emission for transitions between v' and v_2'' vibrational energy levels
J', J''	quantum number of the total angular momentum
K'	quantum number of rotational energy level of $N_2^+B^2\Sigma_u^+$
K_1''	quantum number of rotational energy level of $N_2X^1\Sigma_g^+$
K_2''	quantum number of rotational energy level of $N_2^+X^2\Sigma_g^+$
k	Boltzmann's constant
M', M''	quantum number of a component of total angular momentum
N_n	number density population of state n
N_o	steady-state number density population of $N_2X^1\Sigma_g^+$
$N_{K'}$	steady-state number density population of a rotational energy level K' of $N_2^+B^2\Sigma_u^+$
$N_{v'}$	steady-state number density population of a vibrational energy level v' of $N_2^+B^2\Sigma_u^+$
N_2	neutral nitrogen
N_2^+	ionized nitrogen

$N_2^+B^2\Sigma_u^+$	excited ion state of N_2^+
$N_2X^1\Sigma_g^+$	ground state of N_2
$N_2^+X^2\Sigma_g^+$	ground state of N_2^+
P_R^a	relative rotational line strength for excitation
P_{RR}^a, P_{RP}^a	relative rotational line strength for excitation, R-branch and P-branch, respectively
P_R^e	relative rotational line strength for emission
P_{RR}^e, P_{RP}^e	relative rotational line strength for emission, R-branch and P-branch, respectively
$P_{v'v''}$	band strength
Q_r	rotational partition function
Q_v	vibrational partition function
q	momentum transfer term
$q_{v'v''}$	Franck-Condon factor
R	depopulation rate of $N_2^+B^2\Sigma_u^+$
R_{ij}^e	electronic transition moment for electronic states i and j
$\bar{r}_i$	position vector of ith orbital electron
r_n	nuclei separation
$\bar{r}_1$	position vector of primary electron with respect to point of observation
r_{12}	distance between primary and secondary electrons
r_{1i}	distance between primary and ith orbital electrons
$\bar{r}_2$	position vector of secondary electron with respect to point of observation

$\bar{r}_2'$	position vector of secondary electron with respect to molecular axis
$S_{K''}^{K'}$	Hönl-London factor
T_R	rotational temperature
T_v	vibrational temperature
v	velocity of primary electron
v_o	velocity of atomic electron
v'	vibrational energy state of $N_2^+B^2\Sigma_u^+$
V_o', V_1'	vibrational energy states of $N_2^+B^2\Sigma_u^+$
v_1''	vibrational energy state of $N_2X^1\Sigma_g^+$
v_2''	vibrational energy state of $N_2^+X^2\Sigma_g^+$
X	a constant of $A_{v'K'}$, v_2'' K_2''
$X^1\Sigma_g^+$	represents the electronic wavefunction for $N_2X^1\Sigma_g^+$
Z, Z', Z''	constants defined in the text
θ	scattering angle of primary electron
θ, χ, φ	Euler angles
Λ', Λ''	quantum number of the resultant electronic orbital angular momentum
ν_{nm}	wave number of nm transition
σ_n	excitation cross section
$\sigma_u 2s$	angular characteristics of an orbital electron of $N_2X^1\Sigma_g^+$
ψ_e	electronic state wave function
$\psi_{evJ\Lambda M}$	molecular wave function
$\psi_{J\Lambda M}$	rotational state wave function
ψ_v	vibrational state wave function

REFERENCES

1. Muntz, E. P.: Measurement of Rotational Temperature, Vibrational Temperature, and Molecular Concentration in Non-Radiating Flow of Low Density Nitrogen. University of Toronto, Institute of Aerophysics, Report No. 71, April 1961.
2. Davidson, Gilbert: The Fluorescence of Air and Nitrogen Excited by 50 Kev Electrons. American Science and Engineering, Inc., N65-15109, 1963.
3. Landau, L. D., and Lifshitz, E. M.: Quantum Mechanics: Non-Relativistic Theory. Addison-Wesley, 1958.
4. Richtmyer, F. K., Kennard, E. H., and Lauritsen, T.: Introduction to Modern Physics. McGraw-Hill, 1955.
5. Wannier, G. H.: Physical Review. 90, 817, 1953.
6. Tanaka, T., Namioka, T., and Jursa, A. S.: Canadian Journal of Physics. 39, 1138, 1961.
7. Herzberg, G.: Spectra of Diatomic Molecules. D. Van Nostrand and Co., 1950.
8. Bates, D. R.: Proceedings Royal Society. A196, 217, 1949.
9. Wallace, L. V., and Nicholls, R. W.: Journal of Terrestial Physics. 7, 101, 1955.
10. Gaydon, A. G.: The Spectroscopy of Flame. Chapman and Hall, 1957.
11. Johnson, R. C.: An Introduction to Molecular Spectra. Methuen and Co., 1949.
12. Ocheltree, S. L.: NASA Technical Report. Not released as of this date

VITA

The author was born in South Norfolk, Virginia, on March 26, 1930. He graduated from South Norfolk High School, South Norfolk, Virginia, in June 1948; Newport News Shipbuilding and Dry Dock Company Apprentice School, Newport News, Virginia, in July 1955; and received a Bachelor of Electrical Engineering degree from the University of Virginia, Charlottesville, Virginia, in June 1958. The author entered the graduate school of the College of William and Mary in September 1963. He is presently employed by the National Aeronautics and Space Administration, Langley Research Center, Langley Station, Hampton, Virginia.

TABLE 1.- $\log_{10} \left\{ [G](\nu/\nu_o)^4 \right\}$ VALUES FOR 0-0 BAND

0-0 BAND

T(R) K'	50.0	75.0	100.0	125.0	150.0	175.0	200.0
0.	-0.0507	-0.0341	-0.0258	-0.0208	-0.0175	-0.0151	-0.0133
1.0	-0.0445	-0.0312	-0.0241	-0.0196	-0.0166	-0.0144	-0.0127
2.0	-0.0325	-0.0257	-0.0208	-0.0174	-0.0150	-0.0131	-0.0117
3.0	-0.0152	-0.0178	-0.0162	-0.0144	-0.0127	-0.0114	-0.0103
4.0	0.0073	-0.0073	-0.0102	-0.0104	-0.0099	-0.0092	-0.0085
5.0	0.0343	0.0054	-0.0027	-0.0054	-0.0063	-0.0065	-0.0064
6.0	0.0653	0.0203	0.0060	0.0004	-0.0022	-0.0033	-0.0038
7.0	0.0998	0.0373	0.0161	0.0070	0.0026	0.0003	-0.0010
8.0	0.1372	0.0562	0.0274	0.0145	0.0080	0.0044	0.0023
9.0	0.1772	0.0769	0.0398	0.0229	0.0140	0.0090	0.0059
10.0	0.2192	0.0991	0.0533	0.0320	0.0206	0.0140	0.0099
11.0	0.2630	0.1228	0.0679	0.0418	0.0278	0.0194	0.0142
12.0	0.3081	0.1477	0.0835	0.0524	0.0354	0.0253	0.0188
13.0	0.3544	0.1739	0.1000	0.0638	0.0437	0.0316	0.0239
14.0	0.4016	0.2010	0.1173	0.0757	0.0524	0.0383	0.0292
15.0	0.4496	0.2291	0.1355	0.0883	0.0617	0.0454	0.0348
16.0	0.4981	0.2580	0.1543	0.1015	0.0714	0.0529	0.0408
17.0	0.5471	0.2876	0.1738	0.1152	0.0816	0.0607	0.0471
18.0	0.5965	0.3177	0.1940	0.1295	0.0922	0.0690	0.0536
19.0	0.6462	0.3485	0.2147	0.1443	0.1032	0.0775	0.0605
20.0	0.6961	0.3797	0.2359	0.1595	0.1147	0.0864	0.0677
21.0	0.7462	0.4113	0.2576	0.1752	0.1265	0.0957	0.0751
22.0	0.7964	0.4433	0.2797	0.1913	0.1387	0.1052	0.0828
23.0	0.8468	0.4756	0.3022	0.2077	0.1512	0.1151	0.0908

TABLE 1.- $LOG_{10}\left\{[G](\nu/\nu_o)^4\right\}$ VALUES FOR 0-0 BAND - Continued

0-0 BAND

T(R) K'	225.0	250.0	275.0	300.0	325.0	350.0	400.0
0.	-0.0120	-0.0109	-0.0099	-0.0092	-0.0086	-0.0080	-0.0071
1.0	-0.0114	-0.0103	-0.0095	-0.0088	-0.0081	-0.0076	-0.0068
2.0	-0.0105	-0.0096	-0.0088	-0.0081	-0.0076	-0.0071	-0.0063
3.0	-0.0094	-0.0086	-0.0079	-0.0073	-0.0068	-0.0064	-0.0057
4.0	-0.0079	-0.0073	-0.0068	-0.0064	-0.0060	-0.0056	-0.0050
5.0	-0.0061	-0.0058	-0.0055	-0.0052	-0.0049	-0.0046	-0.0042
6.0	-0.0040	-0.0040	-0.0040	-0.0039	-0.0037	-0.0036	-0.0032
7.0	-0.0017	-0.0021	-0.0023	-0.0024	-0.0024	-0.0023	-0.0022
8.0	0.0010	0.0002	-0.0003	-0.0007	-0.0009	-0.0010	-0.0011
9.0	0.0040	0.0027	0.0018	0.0012	0.0008	0.0005	0.0002
10.0	0.0072	0.0054	0.0041	0.0032	0.0026	0.0021	0.0015
11.0	0.0107	0.0084	0.0067	0.0055	0.0046	0.0039	0.0030
12.0	0.0145	0.0115	0.0094	0.0078	0.0067	0.0058	0.0045
13.0	0.0186	0.0150	0.0124	0.0104	0.0089	0.0078	0.0062
14.0	0.0230	0.0186	0.0155	0.0131	0.0113	0.0100	0.0080
15.0	0.0276	0.0225	0.0188	0.0160	0.0139	0.0122	0.0099
16.0	0.0325	0.0266	0.0223	0.0191	0.0166	0.0147	0.0119
17.0	0.0377	0.0309	0.0260	0.0223	0.0194	0.0172	0.0140
18.0	0.0431	0.0355	0.0299	0.0257	0.0224	0.0199	0.0162
19.0	0.0487	0.0402	0.0340	0.0292	0.0256	0.0227	0.0185
20.0	0.0546	0.0452	0.0382	0.0329	0.0288	0.0256	0.0209
21.0	0.0607	0.0504	0.0427	0.0368	0.0323	0.0287	0.0234
22.0	0.0671	0.0557	0.0473	0.0408	0.0358	0.0318	0.0260
23.0	0.0737	0.0613	0.0521	0.0450	0.0395	0.0351	0.0287

TABLE 1.- $\log_{10}\left\{[G](\nu/\nu_o)^4\right\}$ VALUES FOR 0-0 BAND - Continued

0-0 BAND

T(R) K′	450.0	500.0	550.0	600.0	650.0	700.0	750.0
0.	-0.0064	-0.0059	-0.0054	-0.0050	-0.0047	-0.0045	-0.0042
1.0	-0.0061	-0.0055	-0.0051	-0.0047	-0.0044	-0.0042	-0.0039
2.0	-0.0056	-0.0051	-0.0047	-0.0043	-0.0040	-0.0038	-0.0036
3.0	-0.0051	-0.0046	-0.0042	-0.0039	-0.0036	-0.0034	-0.0032
4.0	-0.0045	-0.0041	-0.0037	-0.0034	-0.0031	-0.0029	-0.0027
5.0	-0.0038	-0.0034	-0.0031	-0.0028	-0.0026	-0.0024	-0.0022
6.0	-0.0030	-0.0027	-0.0024	-0.0022	-0.0020	-0.0018	-0.0017
7.0	-0.0021	-0.0019	-0.0017	-0.0015	-0.0014	-0.0012	-0.0011
8.0	-0.0011	-0.0010	-0.0009	-0.0008	-0.0007	-0.0006	-0.0005
9.0	0.0000	-0.0000	-0.0000	-0.0000	0.0001	0.0001	0.0002
10.0	0.0012	0.0010	0.0009	0.0009	0.0009	0.0009	0.0009
11.0	0.0024	0.0021	0.0019	0.0018	0.0017	0.0017	0.0017
12.0	0.0038	0.0033	0.0030	0.0028	0.0026	0.0025	0.0025
13.0	0.0052	0.0046	0.0041	0.0038	0.0036	0.0034	0.0033
14.0	0.0067	0.0059	0.0053	0.0049	0.0046	0.0044	0.0042
15.0	0.0084	0.0073	0.0066	0.0061	0.0057	0.0054	0.0052
16.0	0.0101	0.0088	0.0079	0.0073	0.0068	0.0065	0.0062
17.0	0.0119	0.0104	0.0093	0.0086	0.0080	0.0076	0.0072
18.0	0.0137	0.0120	0.0108	0.0099	0.0092	0.0087	0.0083
19.0	0.0157	0.0137	0.0123	0.0113	0.0105	0.0099	0.0094
20.0	0.0177	0.0155	0.0139	0.0127	0.0118	0.0111	0.0106
21.0	0.0199	0.0174	0.0156	0.0142	0.0132	0.0124	0.0118
22.0	0.0221	0.0193	0.0173	0.0158	0.0147	0.0138	0.0131
23.0	0.0244	0.0213	0.0191	0.0174	0.0162	0.0152	0.0144

TABLE 1.- $LOG_{10}\left\{[G](\nu/\nu_o)^4\right\}$ VALUES FOR 0-0 BAND - Concluded

	0-0 BAND						
T(R)	800.0	850.0	900.0	950.0	1000.0	1050.0	1100.0
K'							
0.	-0.0040	-0.0038	-0.0037	-0.0035	-0.0034	-0.0033	-0.0032
1.0	-0.0037	-0.0035	-0.0034	-0.0032	-0.0031	-0.0030	-0.0029
2.0	-0.0034	-0.0032	-0.0030	-0.0029	-0.0028	-0.0026	-0.0025
3.0	-0.0030	-0.0028	-0.0027	-0.0025	-0.0024	-0.0023	-0.0022
4.0	-0.0025	-0.0024	-0.0022	-0.0021	-0.0020	-0.0019	-0.0018
5.0	-0.0021	-0.0019	-0.0018	-0.0017	-0.0016	-0.0015	-0.0014
6.0	-0.0015	-0.0014	-0.0013	-0.0012	-0.0011	-0.0010	-0.0009
7.0	-0.0010	-0.0009	-0.0008	-0.0007	-0.0006	-0.0005	-0.0004
8.0	-0.0004	-0.0003	-0.0002	-0.0001	-0.0000	0.0000	0.0001
9.0	0.0003	0.0003	0.0004	0.0005	0.0005	0.0006	0.0006
10.0	0.0009	0.0010	0.0010	0.0011	0.0011	0.0012	0.0012
11.0	0.0017	0.0017	0.0017	0.0017	0.0018	0.0018	0.0018
12.0	0.0024	0.0024	0.0024	0.0024	0.0024	0.0025	0.0025
13.0	0.0033	0.0032	0.0032	0.0032	0.0032	0.0032	0.0032
14.0	0.0041	0.0040	0.0040	0.0039	0.0039	0.0039	0.0039
15.0	0.0050	0.0049	0.0048	0.0047	0.0047	0.0046	0.0046
16.0	0.0060	0.0058	0.0057	0.0056	0.0055	0.0054	0.0054
17.0	0.0070	0.0067	0.0066	0.0065	0.0064	0.0063	0.0062
18.0	0.0080	0.0077	0.0075	0.0074	0.0072	0.0071	0.0070
19.0	0.0091	0.0088	0.0085	0.0083	0.0082	0.0080	0.0079
20.0	0.0102	0.0098	0.0095	0.0093	0.0091	0.0089	0.0088
21.0	0.0113	0.0109	0.0106	0.0103	0.0101	0.0099	0.0097
22.0	0.0125	0.0120	0.0117	0.0114	0.0111	0.0109	0.0107
23.0	0.0137	0.0132	0.0128	0.0125	0.0122	0.0119	0.0117

TABLE 2.- $\log_{10}\left\{[G](\nu/\nu_o)^4\right\}$ VALUES FOR 0-1 BAND

0-1 BAND

T(R) K′	50.0	75.0	100.0	125.0	150.0	175.0	200.0
0.	-0.0507	-0.0342	-0.0259	-0.0209	-0.0176	-0.0152	-0.0134
1.0	-0.0446	-0.0313	-0.0241	-0.0197	-0.0166	-0.0144	-0.0128
2.0	-0.0326	-0.0258	-0.0209	-0.0175	-0.0150	-0.0132	-0.0117
3.0	-0.0152	-0.0178	-0.0162	-0.0144	-0.0127	-0.0114	-0.0103
4.0	0.0073	-0.0073	-0.0101	-0.0103	-0.0098	-0.0091	-0.0085
5.0	0.0344	0.0055	-0.0026	-0.0054	-0.0062	-0.0064	-0.0063
6.0	0.0654	0.0205	0.0062	0.0005	-0.0020	-0.0032	-0.0037
7.0	0.0999	0.0375	0.0163	0.0072	0.0028	0.0005	-0.0008
8.0	0.1375	0.0565	0.0276	0.0148	0.0083	0.0047	0.0026
9.0	0.1775	0.0772	0.0401	0.0232	0.0144	0.0093	0.0062
10.0	0.2196	0.0995	0.0537	0.0324	0.0210	0.0144	0.0103
11.0	0.2635	0.1232	0.0684	0.0423	0.0282	0.0199	0.0147
12.0	0.3087	0.1483	0.0841	0.0530	0.0360	0.0259	0.0194
13.0	0.3551	0.1745	0.1006	0.0644	0.0443	0.0322	0.0245
14.0	0.4024	0.2018	0.1181	0.0764	0.0532	0.0390	0.0299
15.0	0.4504	0.2299	0.1363	0.0891	0.0625	0.0462	0.0356
16.0	0.4990	0.2588	0.1552	0.1023	0.0723	0.0538	0.0417
17.0	0.5481	0.2886	0.1749	0.1162	0.0826	0.0618	0.0481
18.0	0.5976	0.3189	0.1951	0.1306	0.0933	0.0701	0.0548
19.0	0.6474	0.3497	0.2159	0.1455	0.1045	0.0788	0.0617
20.0	0.6974	0.3811	0.2372	0.1608	0.1160	0.0878	0.0690
21.0	0.7476	0.4128	0.2590	0.1766	0.1280	0.0972	0.0766
22.0	0.7980	0.4449	0.2813	0.1929	0.1403	0.1069	0.0844
23.0	0.8485	0.4773	0.3039	0.2095	0.1530	0.1168	0.0925

TABLE 2.- $LOG_{10}\left\{[G](\nu/\nu_o)^4\right\}$ VALUES FOR 0-1 BAND - Continued

0-1 BAND

T(R) K'	225.0	250.0	275.0	300.0	325.0	350.0	400.0
0.	-0.0120	-0.0109	-0.0100	-0.0093	-0.0086	-0.0081	-0.0072
1.0	-0.0115	-0.0104	-0.0096	-0.0088	-0.0082	-0.0077	-0.0068
2.0	-0.0106	-0.0096	-0.0088	-0.0082	-0.0076	-0.0071	-0.0063
3.0	-0.0094	-0.0086	-0.0079	-0.0073	-0.0068	-0.0064	-0.0057
4.0	-0.0078	-0.0073	-0.0068	-0.0063	-0.0059	-0.0056	-0.0049
5.0	-0.0060	-0.0057	-0.0054	-0.0051	-0.0048	-0.0046	-0.0041
6.0	-0.0039	-0.0039	-0.0038	-0.0037	-0.0036	-0.0034	-0.0031
7.0	-0.0015	-0.0019	-0.0021	-0.0022	-0.0022	-0.0022	-0.0020
8.0	0.0013	0.0004	-0.0001	-0.0004	-0.0006	-0.0007	-0.0008
9.0	0.0043	0.0030	0.0021	0.0015	0.0011	0.0008	0.0005
10.0	0.0076	0.0058	0.0045	0.0036	0.0030	0.0025	0.0019
11.0	0.0112	0.0088	0.0071	0.0059	0.0050	0.0043	0.0034
12.0	0.0151	0.0121	0.0100	0.0084	0.0072	0.0063	0.0051
13.0	0.0193	0.0156	0.0130	0.0110	0.0096	0.0084	0.0069
14.0	0.0237	0.0194	0.0162	0.0138	0.0121	0.0107	0.0087
15.0	0.0284	0.0233	0.0196	0.0168	0.0147	0.0131	0.0107
16.0	0.0334	0.0275	0.0232	0.0199	0.0175	0.0155	0.0128
17.0	0.0387	0.0320	0.0270	0.0233	0.0205	0.0182	0.0150
18.0	0.0442	0.0366	0.0310	0.0268	0.0236	0.0210	0.0173
19.0	0.0499	0.0415	0.0352	0.0305	0.0268	0.0239	0.0197
20.0	0.0560	0.0466	0.0396	0.0343	0.0302	0.0270	0.0223
21.0	0.0622	0.0518	0.0441	0.0383	0.0337	0.0301	0.0249
22.0	0.0687	0.0573	0.0489	0.0424	0.0374	0.0334	0.0276
23.0	0.0754	0.0630	0.0538	0.0467	0.0412	0.0369	0.0305

TABLE 2.- $LOG_{10}\left\{[G](\nu/\nu_o)^4\right\}$ VALUES FOR 0-1 BAND - Continued

0-1 BAND

T(R) K′	450.0	500.0	550.0	600.0	650.0	700.0	750.0
0.	-0.0065	-0.0060	-0.0055	-0.0051	-0.0048	-0.0045	-0.0043
1.0	-0.0062	-0.0056	-0.0052	-0.0048	-0.0045	-0.0042	-0.0040
2.0	-0.0057	-0.0052	-0.0047	-0.0044	-0.0041	-0.0038	-0.0036
3.0	-0.0051	-0.0046	-0.0042	-0.0039	-0.0036	-0.0034	-0.0032
4.0	-0.0044	-0.0040	-0.0037	-0.0034	-0.0031	-0.0029	-0.0027
5.0	-0.0037	-0.0033	-0.0030	-0.0028	-0.0025	-0.0023	-0.0021
6.0	-0.0028	-0.0025	-0.0023	-0.0021	-0.0019	-0.0017	-0.0016
7.0	-0.0019	-0.0017	-0.0015	-0.0014	-0.0012	-0.0011	-0.0009
8.0	-0.0008	-0.0007	-0.0007	-0.0005	-0.0004	-0.0003	-0.0002
9.0	0.0003	0.0003	0.0003	0.0003	0.0004	0.0004	0.0005
10.0	0.0016	0.0014	0.0013	0.0013	0.0013	0.0013	0.0013
11.0	0.0029	0.0026	0.0024	0.0023	0.0022	0.0022	0.0021
12.0	0.0043	0.0038	0.0035	0.0033	0.0032	0.0031	0.0030
13.0	0.0058	0.0052	0.0047	0.0044	0.0042	0.0041	0.0040
14.0	0.0075	0.0066	0.0060	0.0056	0.0053	0.0051	0.0050
15.0	0.0092	0.0081	0.0074	0.0069	0.0065	0.0062	0.0060
16.0	0.0109	0.0097	0.0088	0.0081	0.0077	0.0073	0.0070
17.0	0.0129	0.0114	0.0103	0.0096	0.0090	0.0086	0.0082
18.0	0.0149	0.0131	0.0119	0.0110	0.0103	0.0098	0.0094
19.0	0.0169	0.0150	0.0136	0.0125	0.0117	0.0111	0.0107
20.0	0.0191	0.0169	0.0153	0.0141	0.0132	0.0125	0.0120
21.0	0.0213	0.0189	0.0171	0.0157	0.0147	0.0139	0.0133
22.0	0.0237	0.0209	0.0189	0.0174	0.0163	0.0154	0.0147
23.0	0.0262	0.0231	0.0209	0.0192	0.0179	0.0169	0.0161

TABLE 2.- $\log_{10}\left\{[G](\nu/\nu_o)^4\right\}$ VALUES FOR 0-1 BAND - Concluded

	0-1 BAND						
T(R)	800.0	850.0	900.0	950.0	1000.0	1050.0	1100.0
K'							
0.	-0.0041	-0.0039	-0.0038	-0.0036	-0.0035	-0.0034	-0.0033
1.0	-0.0038	-0.0036	-0.0034	-0.0033	-0.0032	-0.0031	-0.0029
2.0	-0.0034	-0.0032	-0.0031	-0.0029	-0.0028	-0.0027	-0.0026
3.0	-0.0030	-0.0028	-0.0027	-0.0025	-0.0024	-0.0023	-0.0022
4.0	-0.0025	-0.0023	-0.0022	-0.0021	-0.0020	-0.0019	-0.0018
5.0	-0.0020	-0.0018	-0.0017	-0.0016	-0.0015	-0.0014	-0.0013
6.0	-0.0014	-0.0013	-0.0012	-0.0011	-0.0010	-0.0009	-0.0008
7.0	-0.0008	-0.0007	-0.0006	-0.0005	-0.0004	-0.0003	-0.0002
8.0	-0.0001	-0.0000	0.0000	0.0001	0.0002	0.0003	0.0003
9.0	0.0006	0.0007	0.0007	0.0008	0.0008	0.0009	0.0010
10.0	0.0013	0.0014	0.0014	0.0015	0.0015	0.0016	0.0016
11.0	0.0021	0.0022	0.0022	0.0022	0.0022	0.0023	0.0023
12.0	0.0030	0.0030	0.0030	0.0030	0.0030	0.0030	0.0030
13.0	0.0039	0.0038	0.0038	0.0038	0.0038	0.0038	0.0038
14.0	0.0048	0.0048	0.0047	0.0047	0.0046	0.0046	0.0046
15.0	0.0058	0.0057	0.0056	0.0056	0.0055	0.0055	0.0054
16.0	0.0068	0.0067	0.0065	0.0064	0.0064	0.0063	0.0063
17.0	0.0080	0.0078	0.0076	0.0075	0.0074	0.0073	0.0072
18.0	0.0091	0.0088	0.0086	0.0085	0.0084	0.0082	0.0082
19.0	0.0103	0.0100	0.0097	0.0095	0.0094	0.0093	0.0091
20.0	0.0115	0.0112	0.0109	0.0107	0.0105	0.0103	0.0102
21.0	0.0128	0.0124	0.0121	0.0118	0.0116	0.0114	0.0112
22.0	0.0141	0.0137	0.0133	0.0130	0.0127	0.0125	0.0123
23.0	0.0155	0.0150	0.0145	0.0142	0.0139	0.0137	0.0134

TABLE 3.- WEIGHTED MEAN VALUES OF T_R MEASUREMENTS FOR 0-0 BAND

Measured T_R	Weighted mean value of T_R	Inner cylinder reference temperature
317 ±1° K 316 ±2° K	317 ±1° K	297 ±10° K
423 ±2° K 424 ±4° K	423 ±1° K	402 ±13° K
524 ±1° K 511 ±3° K	523 ±4° K	499 ±14° K
616 ±2° K 631 ±5° K	618 ±5° K	618 ±17° K
716 ±2° K 727 ±6° K	717 ±3° K	716 ±18° K
799 ±5° K 808 ±4° K	804 ±4° K	815 ±20° K
886 ±5° K 860 ±7° K	877 ±12° K	898 ±22° K
942 ±4° K 970 ±9° K	947 ±10° K	994 ±24° K
1035 ±2° K 974 ±5° K	1026 ±7° K	1092 ±24° K

TABLE 4.- WEIGHTED MEAN VALUES OF T_R MEASUREMENTS FOR 0-1 BAND

Measured T_R	Weighted mean value of T_R	Inner cylinder reference temperature
320 ±3° K 320 ±5° K	320 ±0° K	297 ±10° K
419 ±1° K 422 ±4° K	419 ±3° K	402 ±13° K
504 ±2° K 482 ±10° K	503 ±4° K	499 ±14° K
626 ±3° K 633 ±5° K	628 ±3° K	618 ±17° K
729 ±7° K 700 ±6° K	712 ±14° K	716 ±18° K
798 ±4° K 781 ±3° K	787 ±3° K	815 ±20° K
862 ±8° K 826 ±4° K	833 ±14° K	898 ±22° K
998 ±4° K 972 ±12° K	995 ±8° K	994 ±24° K
1147 ±38° K 1060 ±8° K	1065 ±25° K	1092 ±24° K

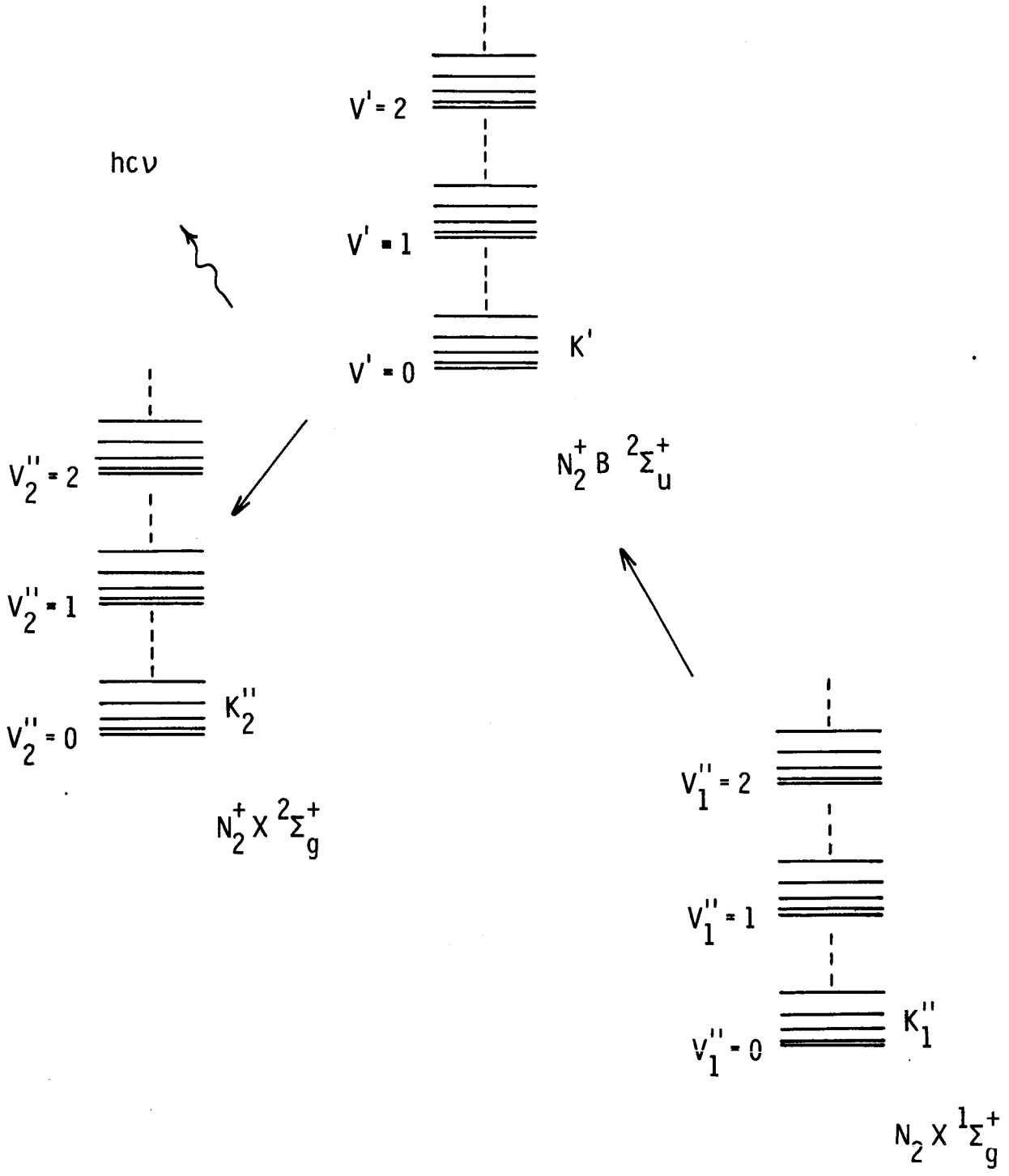

Figure 1.- Partial energy level diagram of nitrogen for high-energy electron beam excitation-emission process.

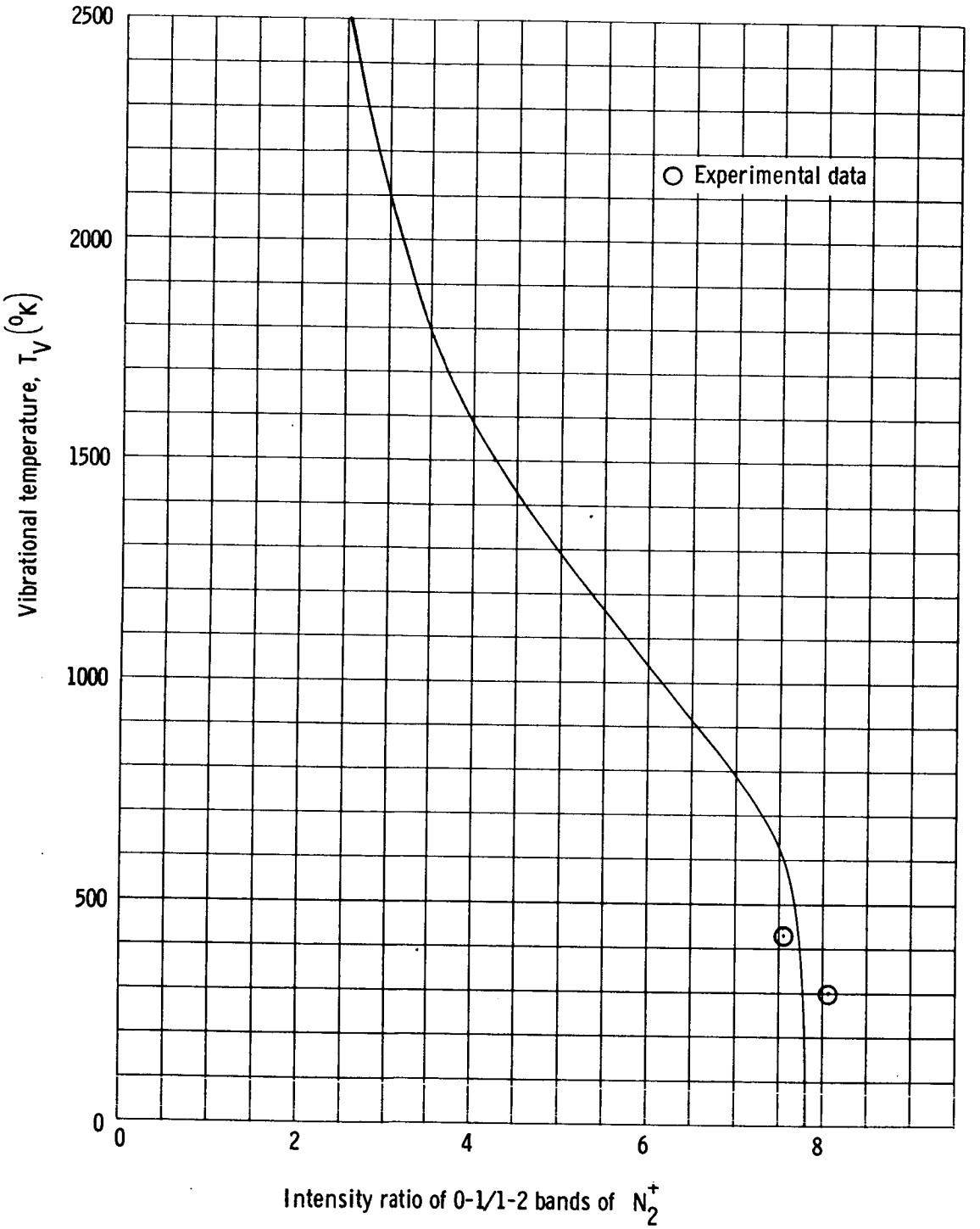

Figure 2.– Graph of vibrational temperature versus intensity ratio of 0-1 and 1-2 bands of N_2^+.

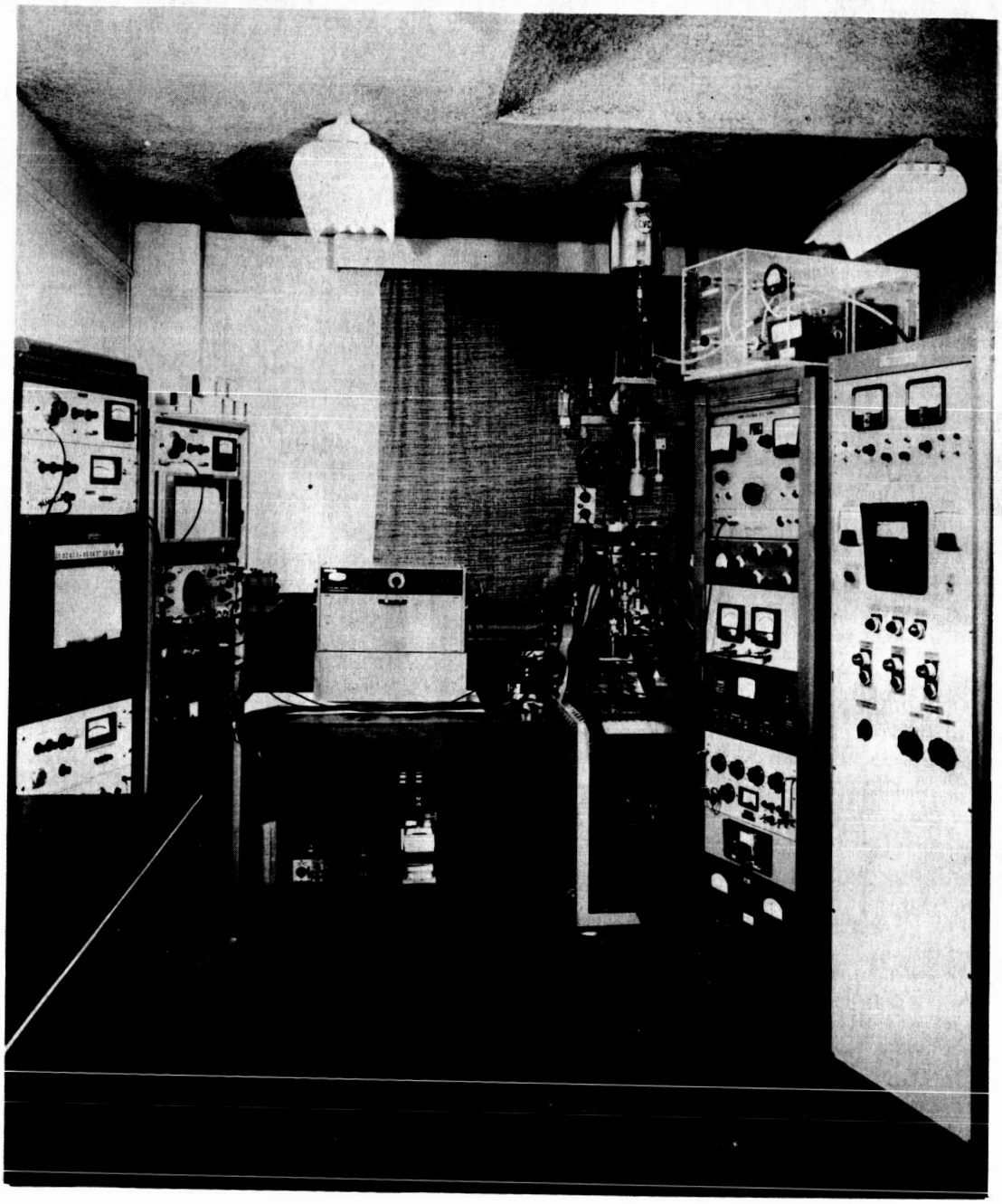

Figure 3.- Experimental system.

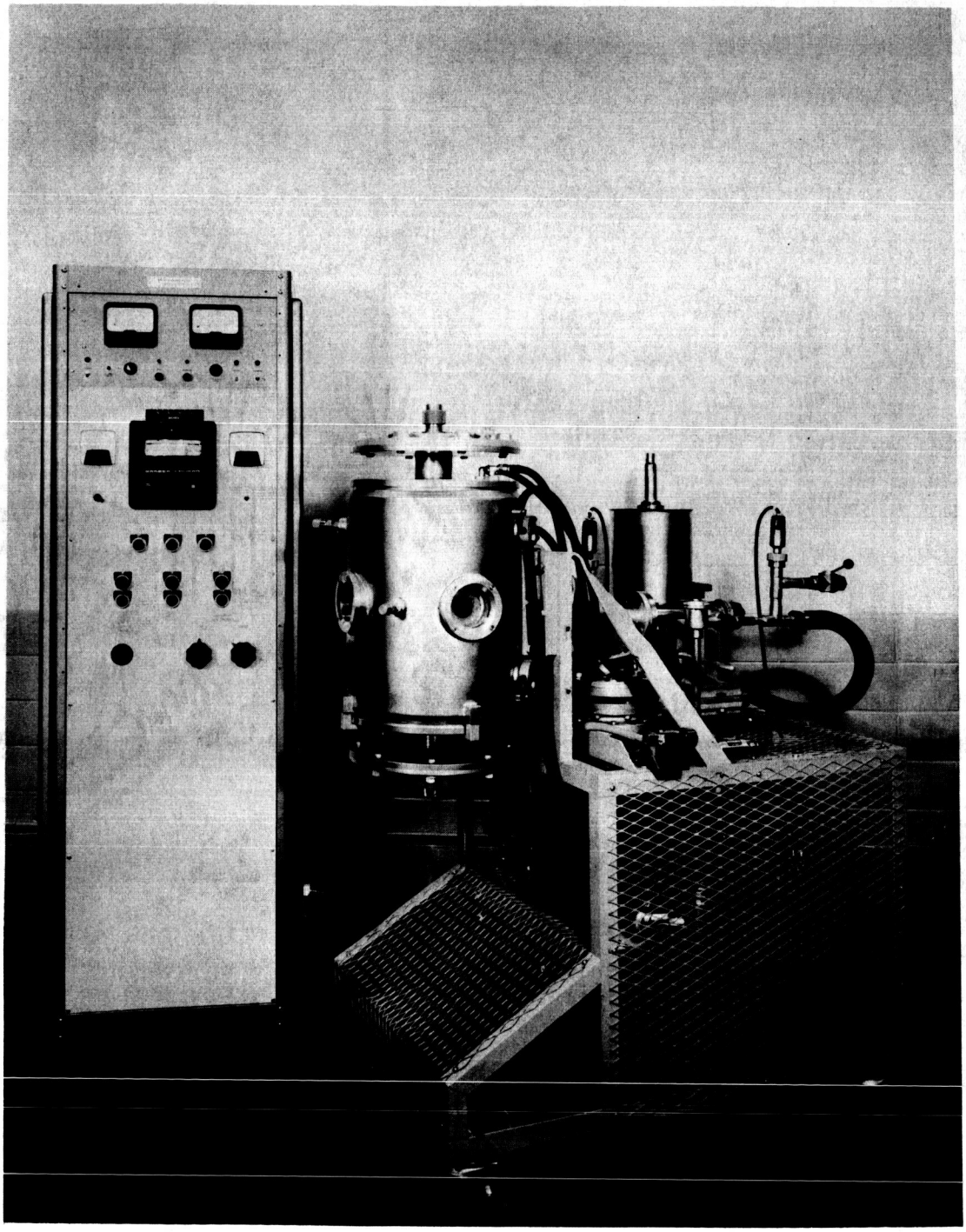

Figure 4.- Test gas temperature and vacuum control system.

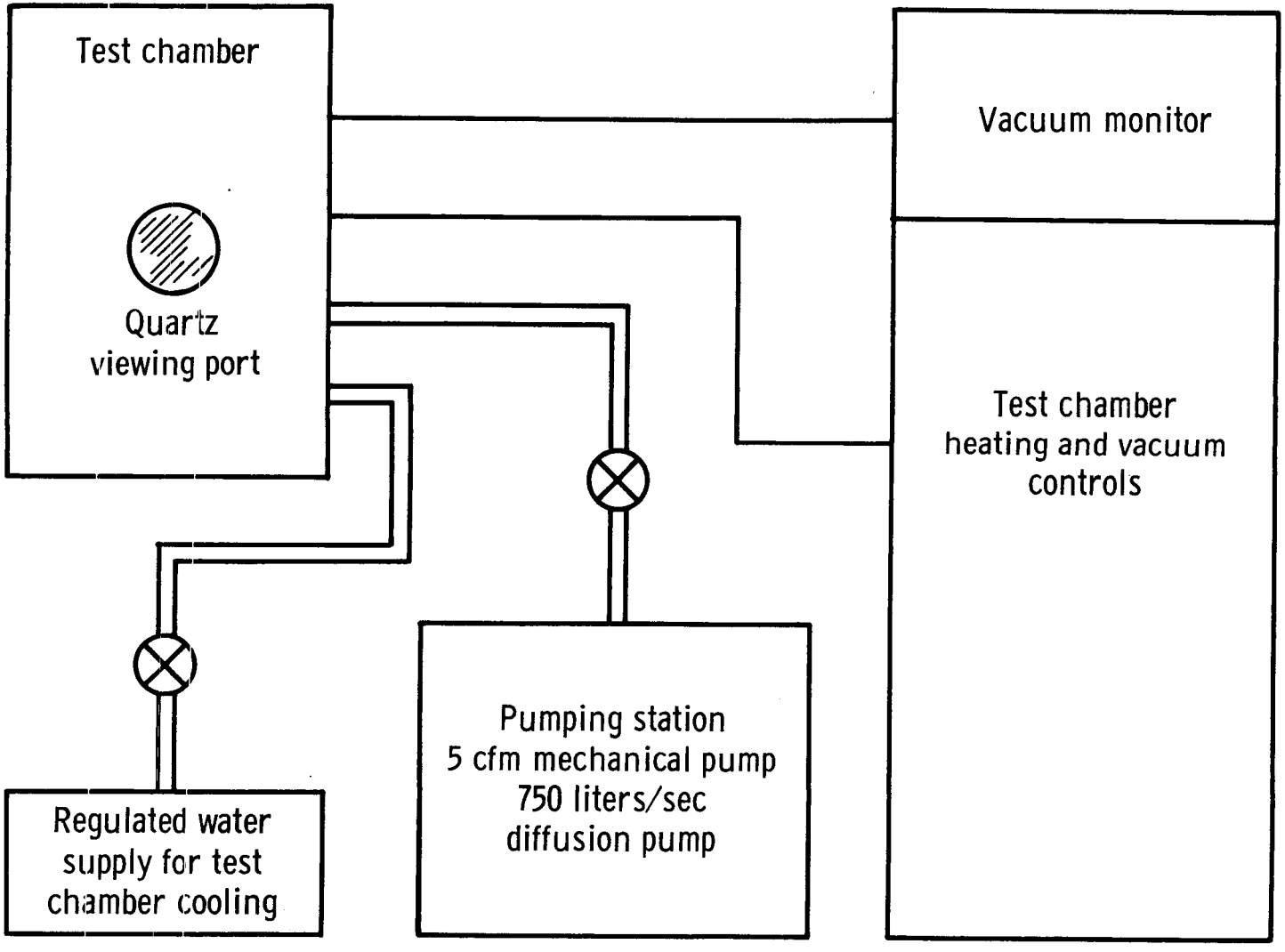

Figure 5.– Block diagram, test gas temperature and vacuum control system.

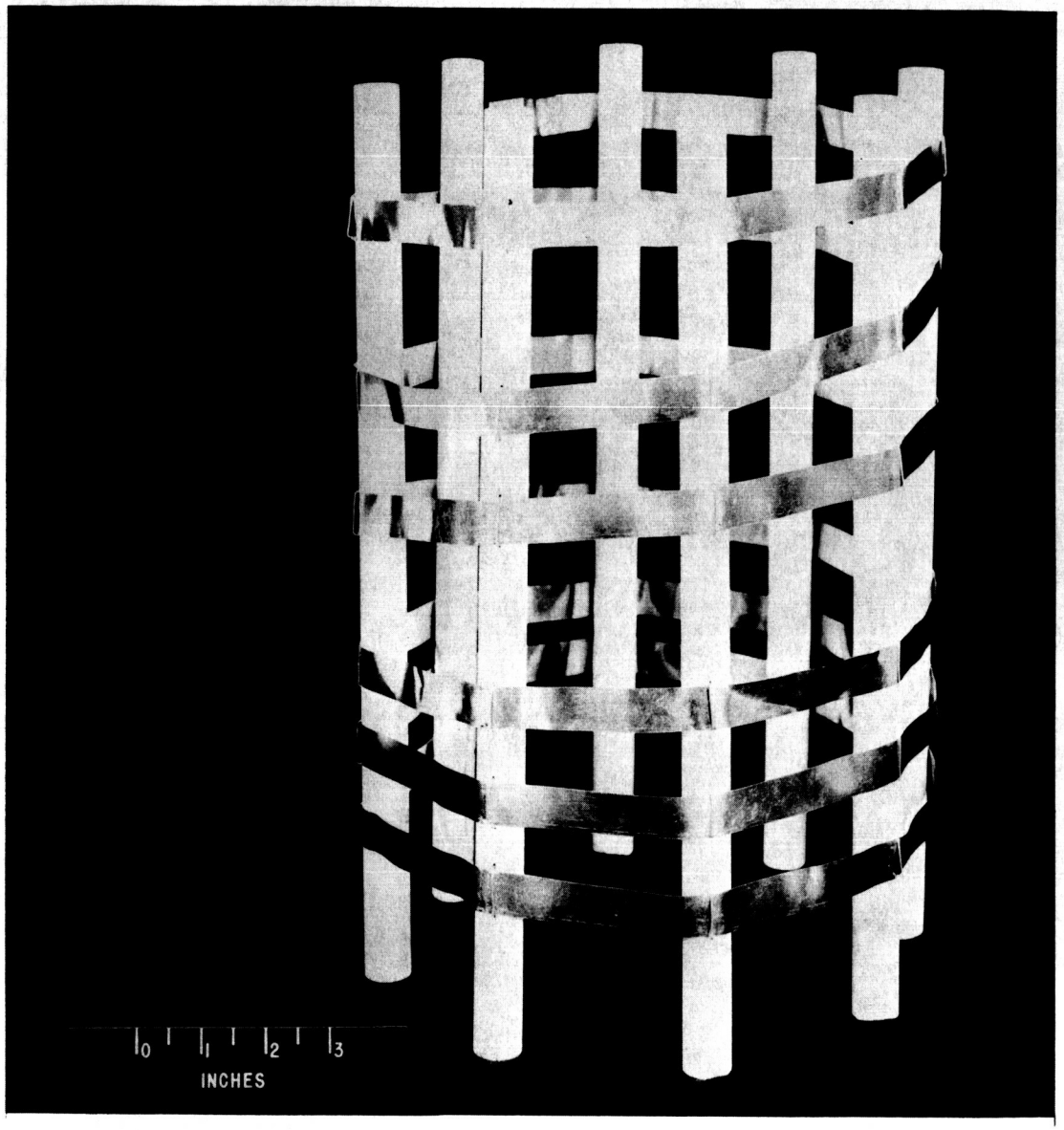

Figure 6.- Test chamber heating element.

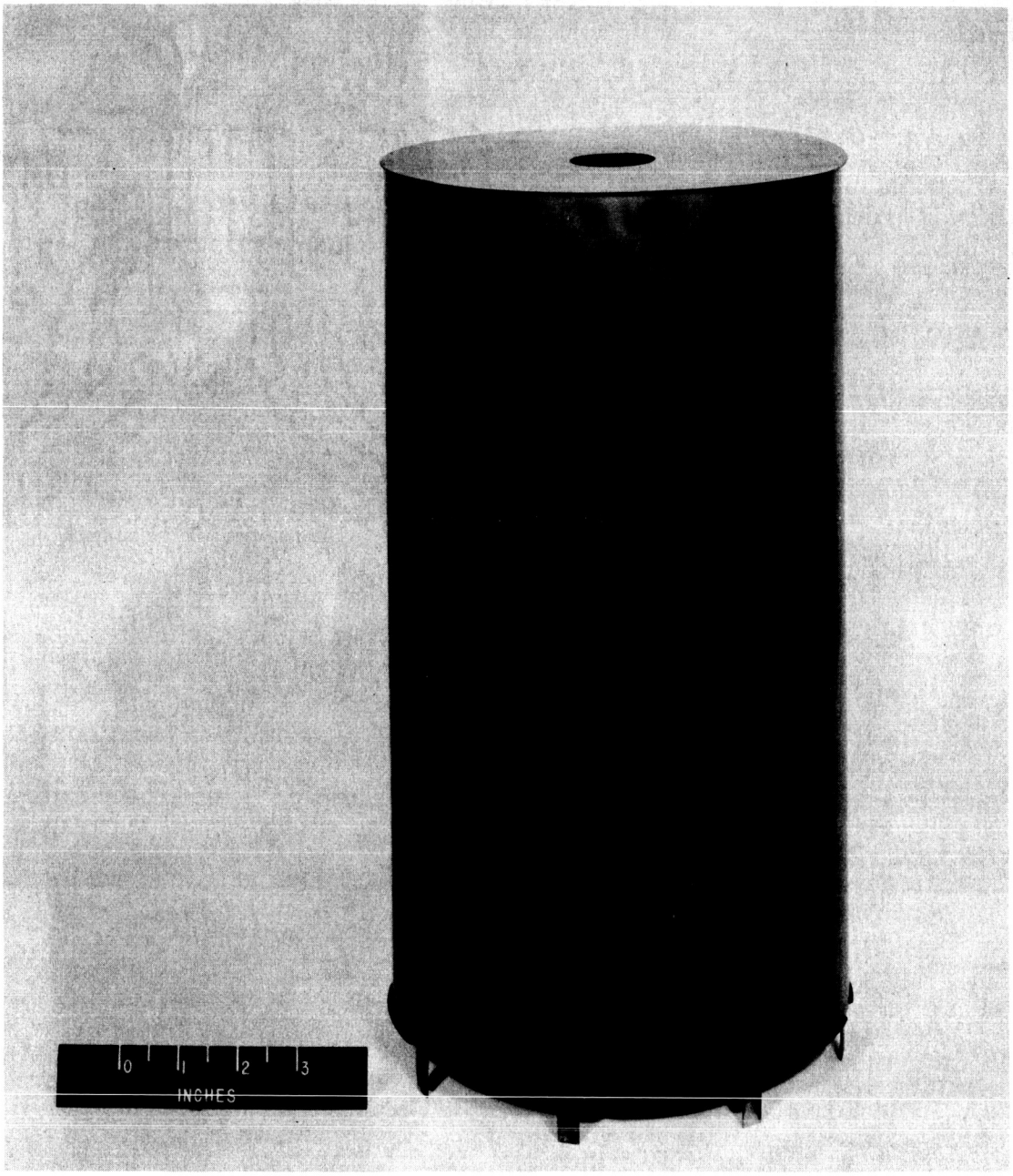

Figure 7.- Test chamber inner cylinder.

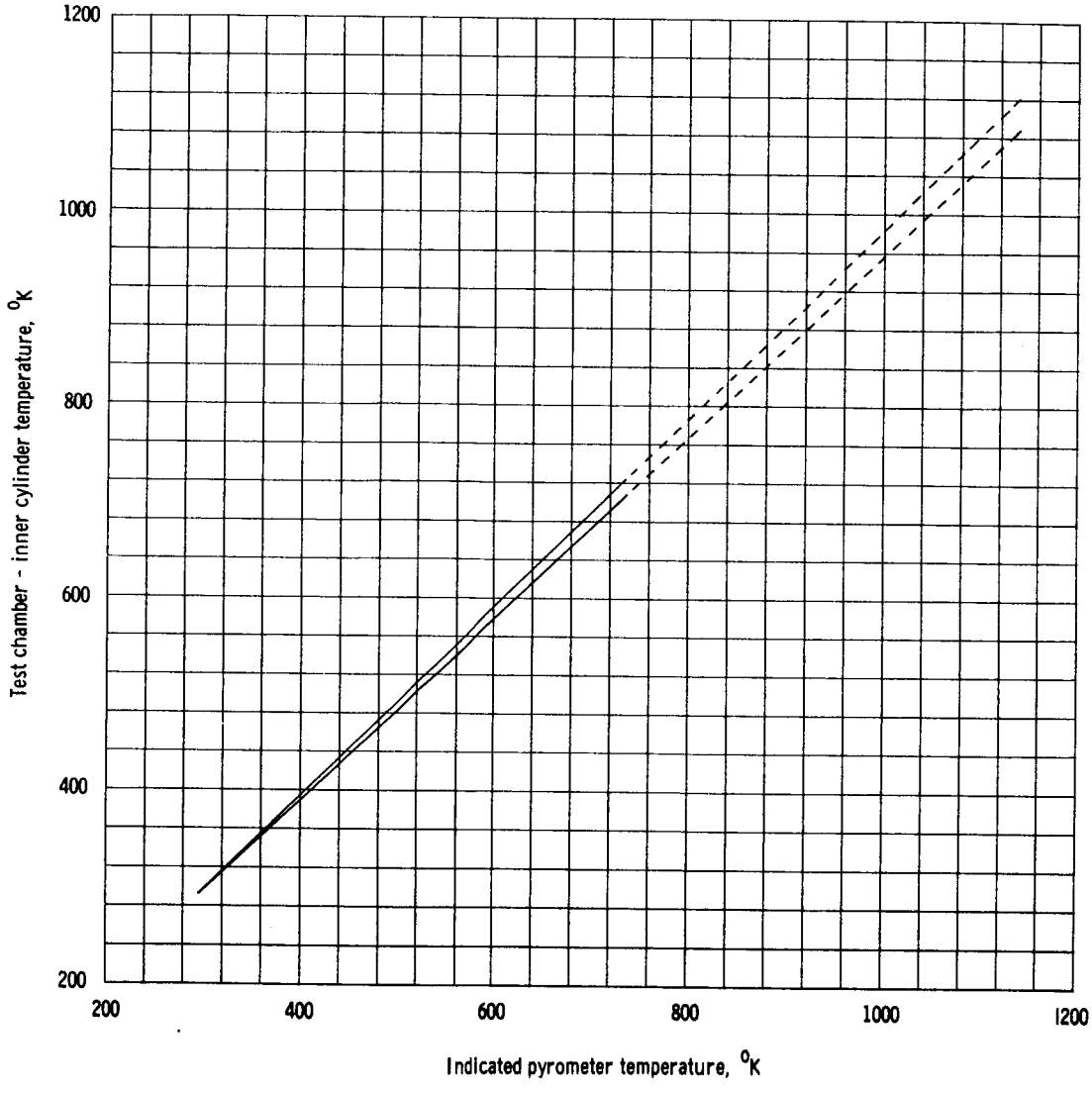

Figure 8.- Graph of test chamber, inner cylinder temperature versus indicated pyrometer temperature.

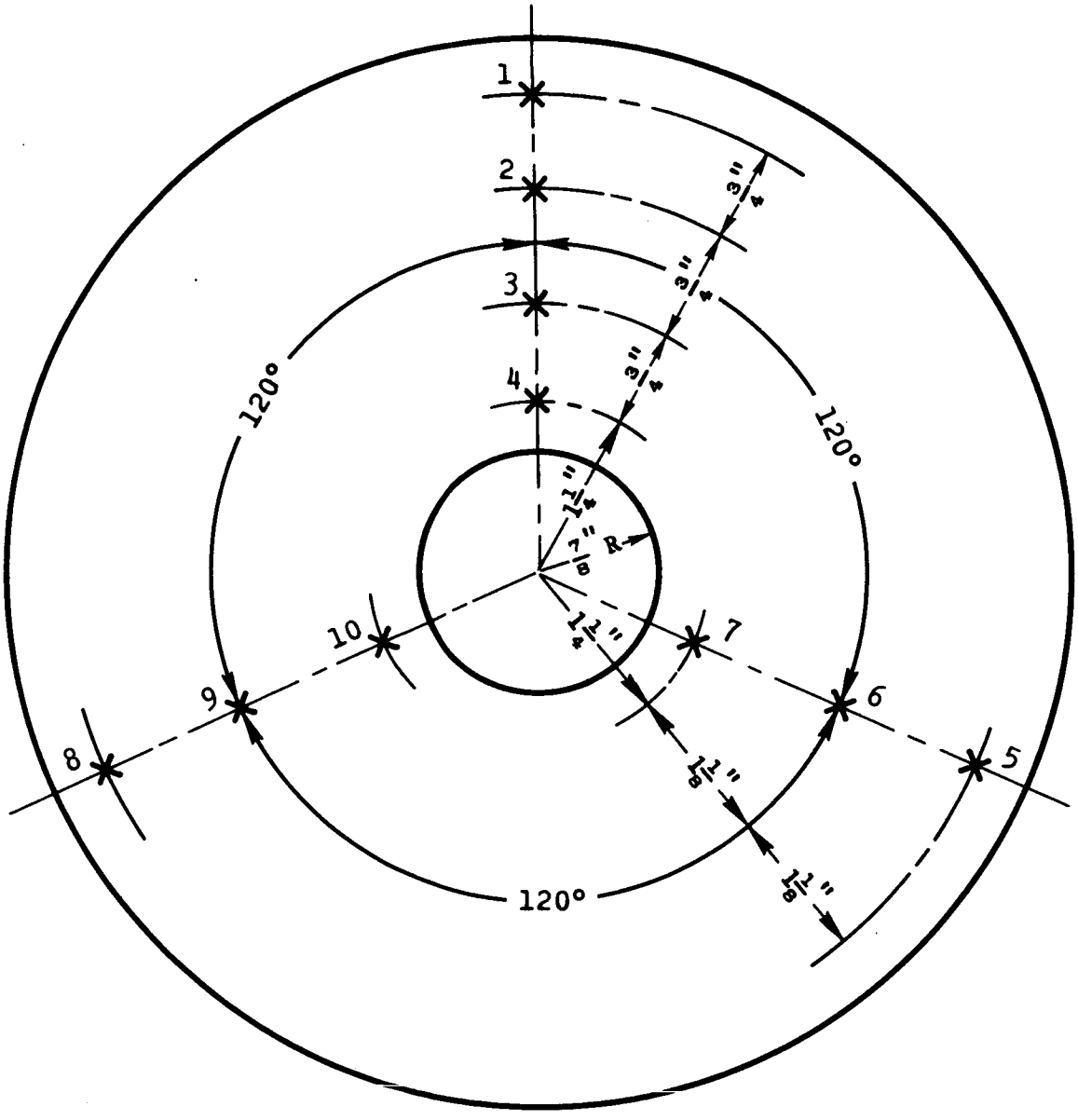

Figure 9.- Inner cylinder, bottom plate thermocouple locations.

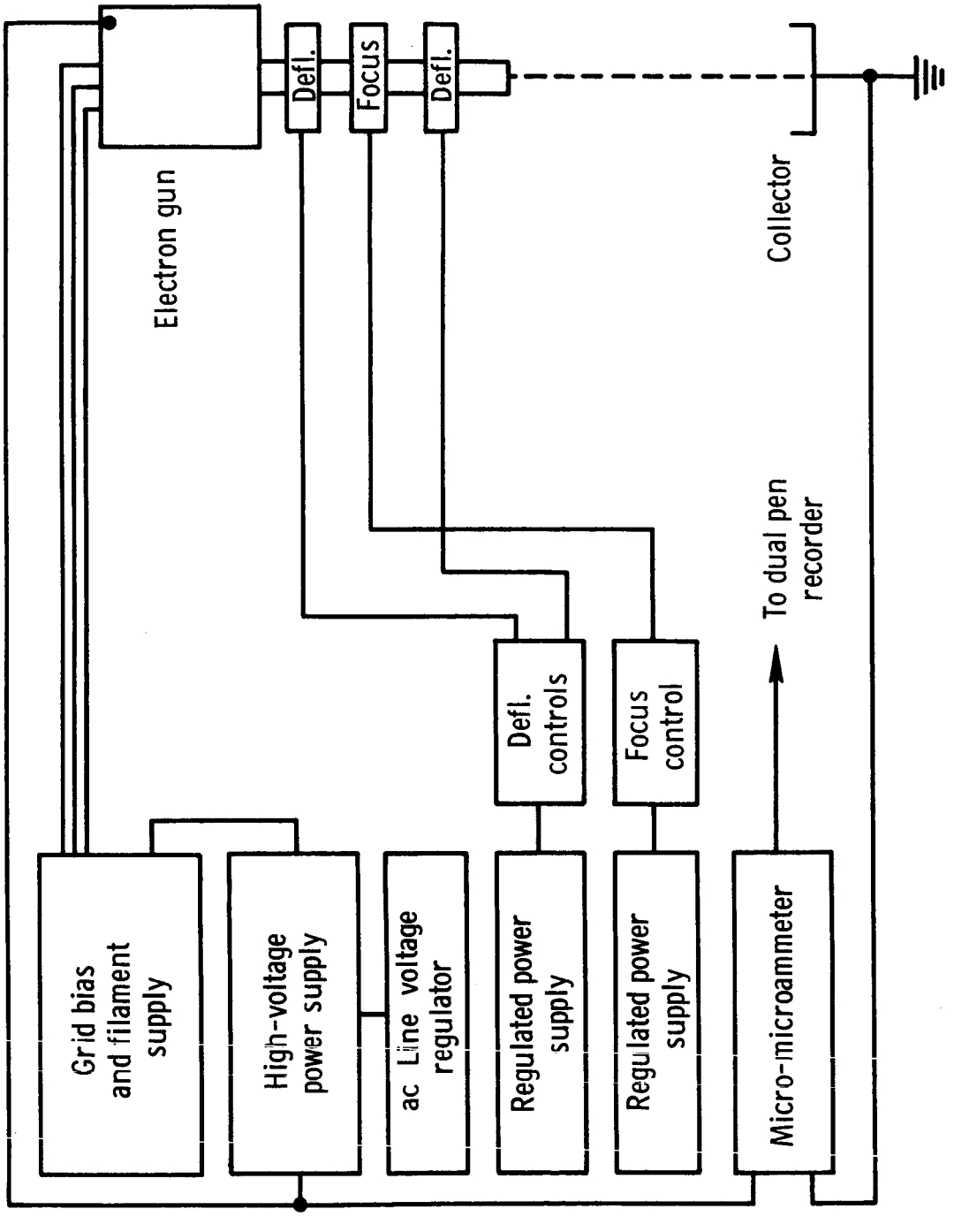

Figure 10.- Block diagram, electron beam system.

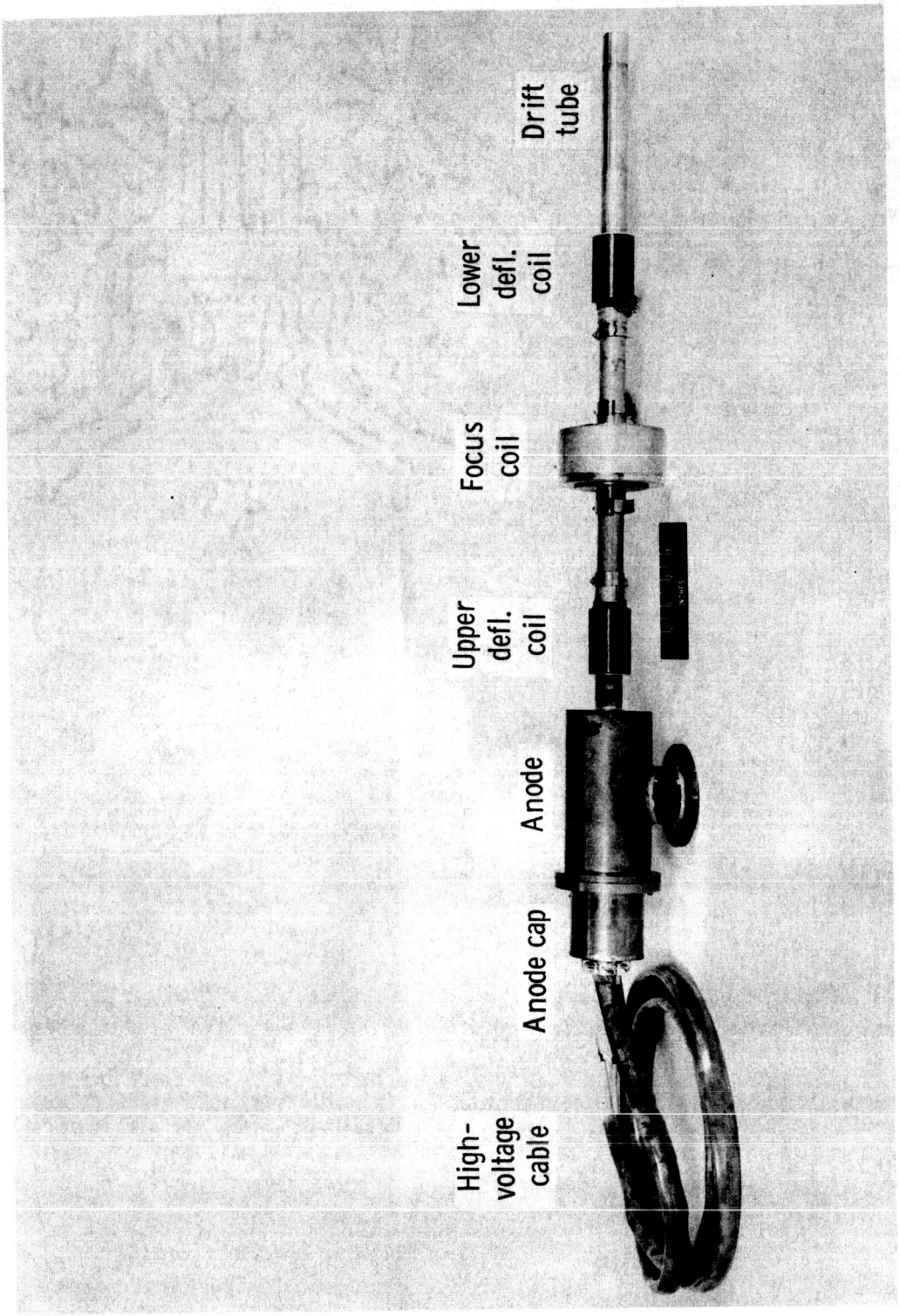

Figure 11.- Electron gun and anode assembly.

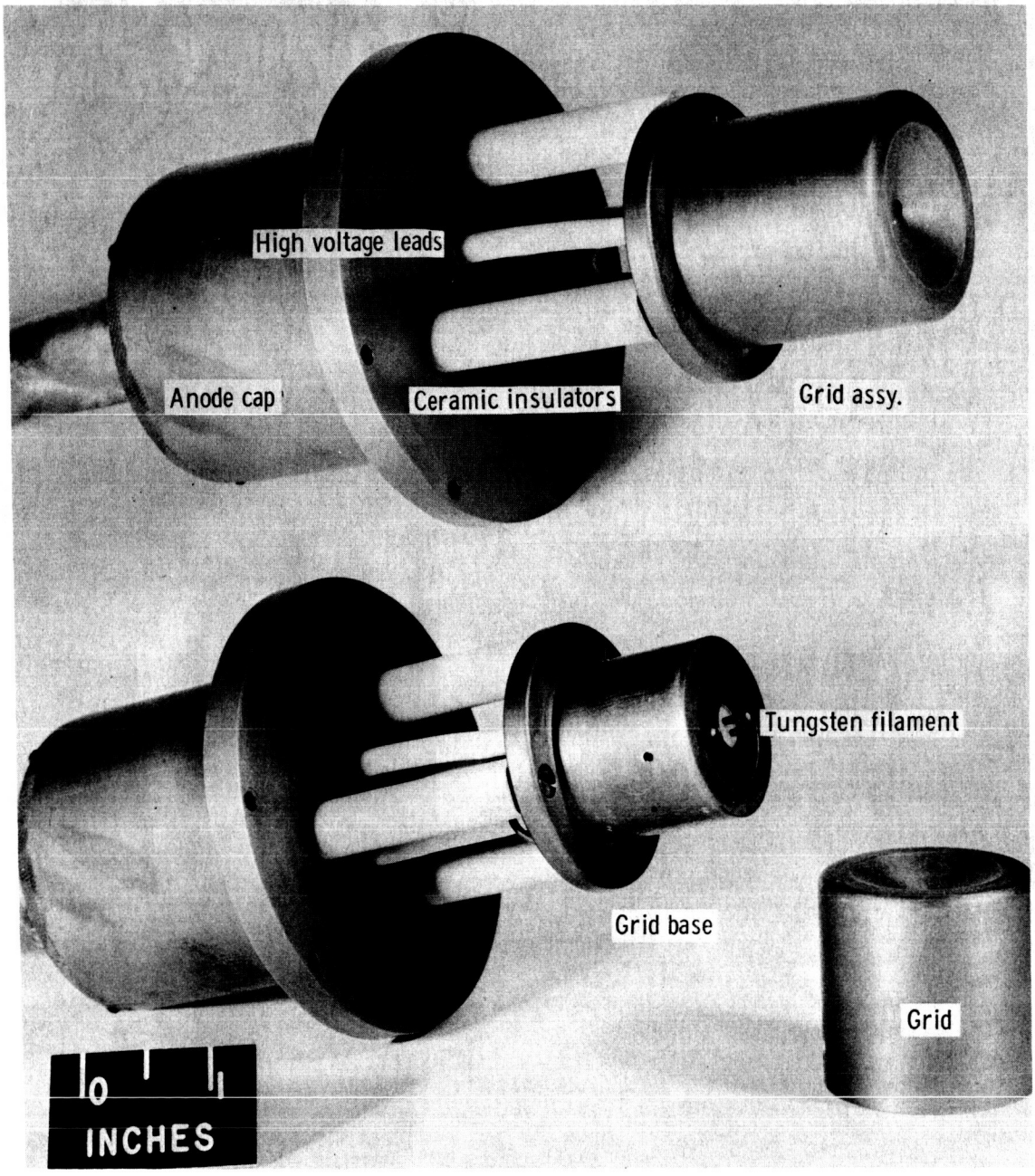

Figure 12.- Electron gun.

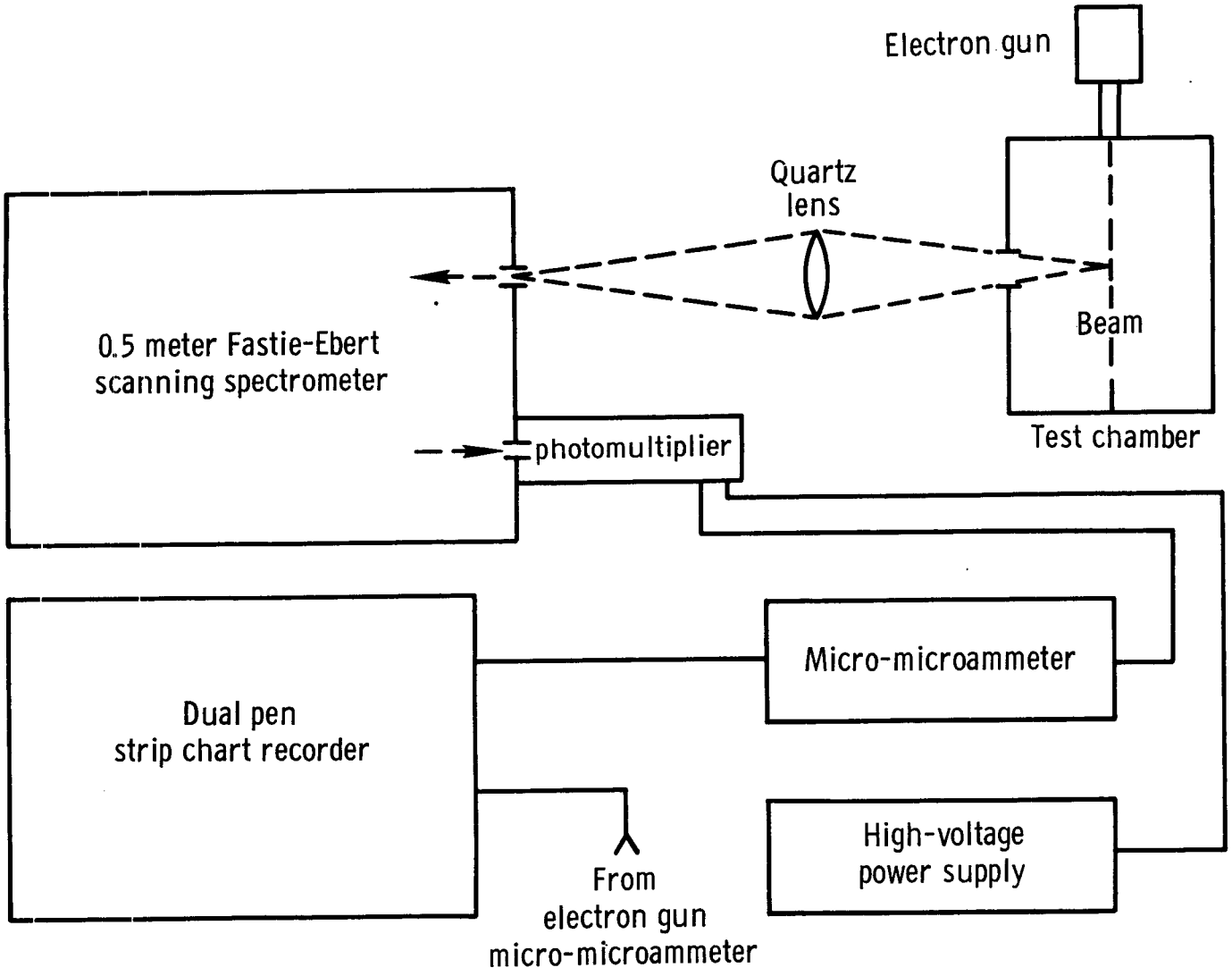

Figure 13.- Block diagram, optical and electronic detector system.

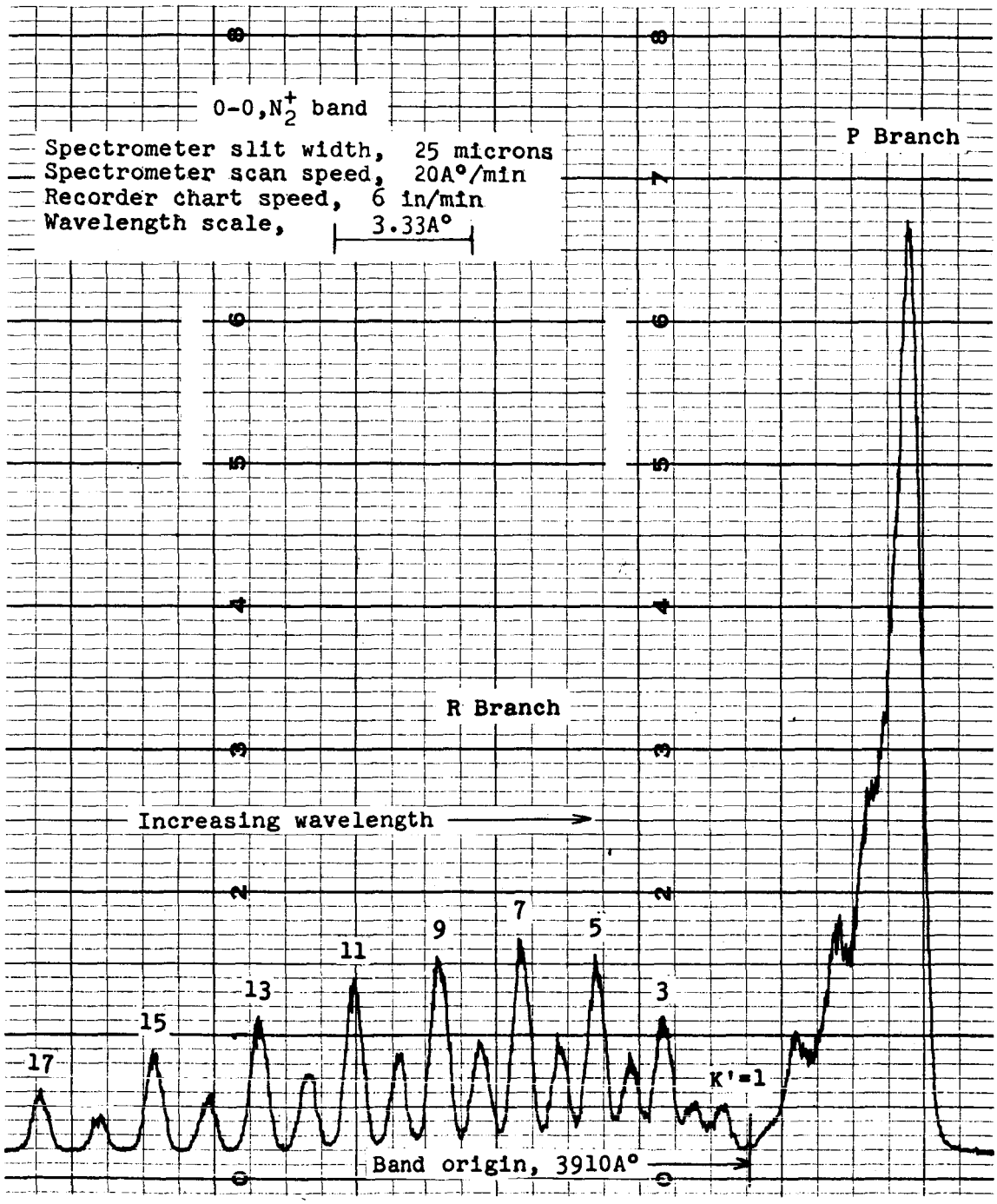

Figure 14.– A spectrometer trace N_2^+ 0-0 band rotational structure, ≈ 300° K.

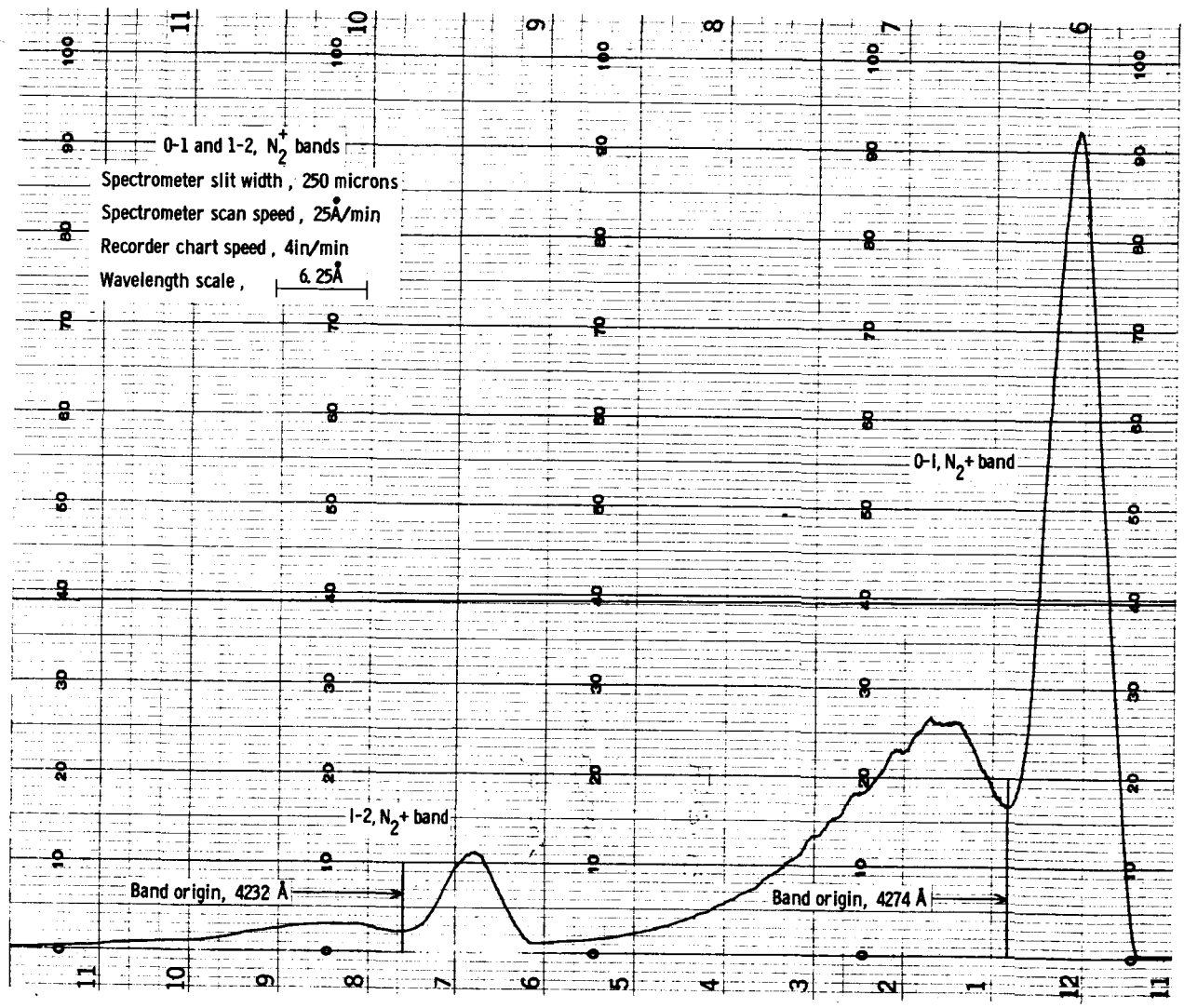

Figure 15.- Typical spectrometer trace unresolved, N_2^+ 0-1 and 1-2 bands, $\approx 300^\circ$ K.

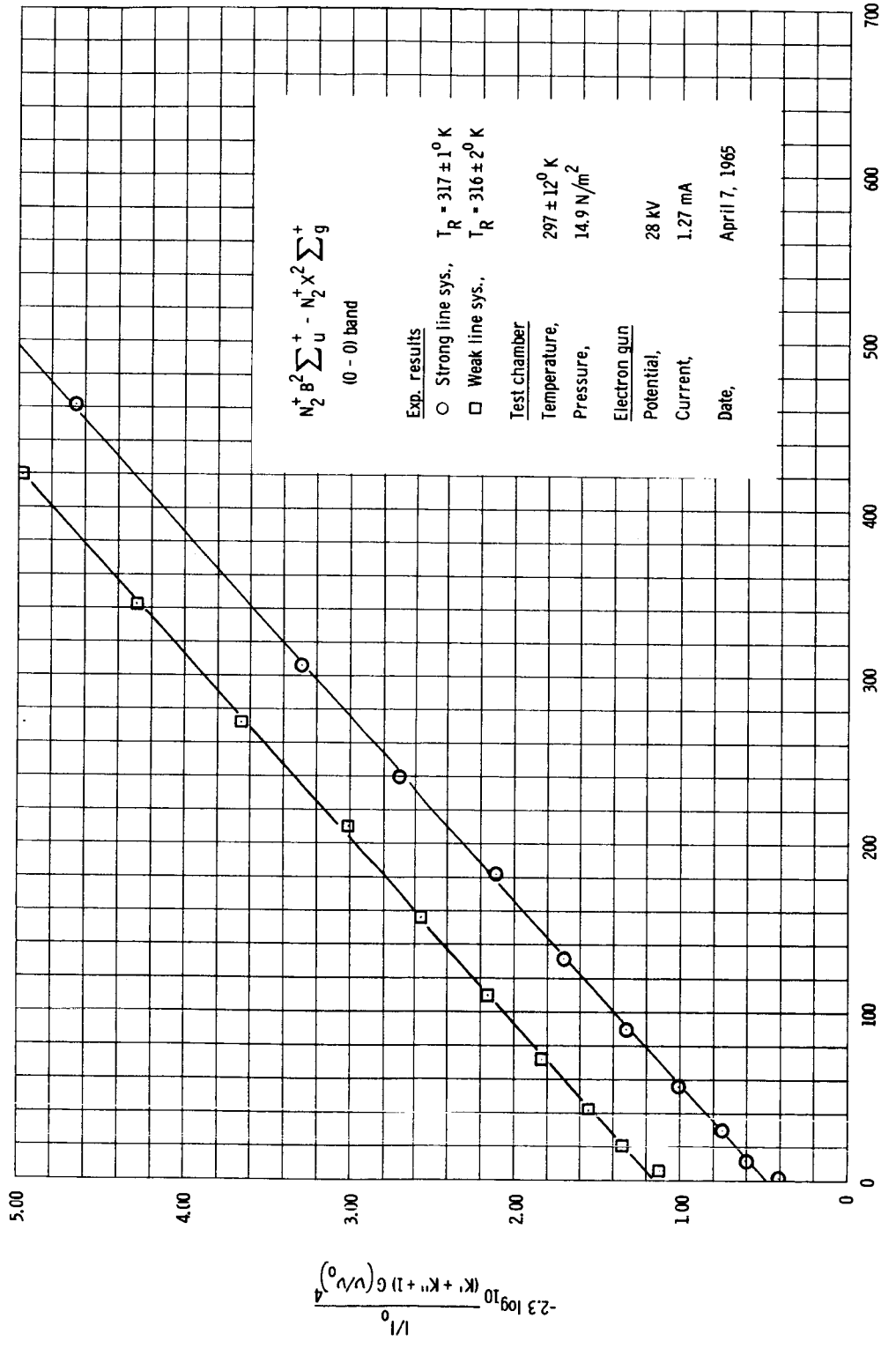

Figure 16.- 0-0 band data for 300° K experiment for T_R measurements.

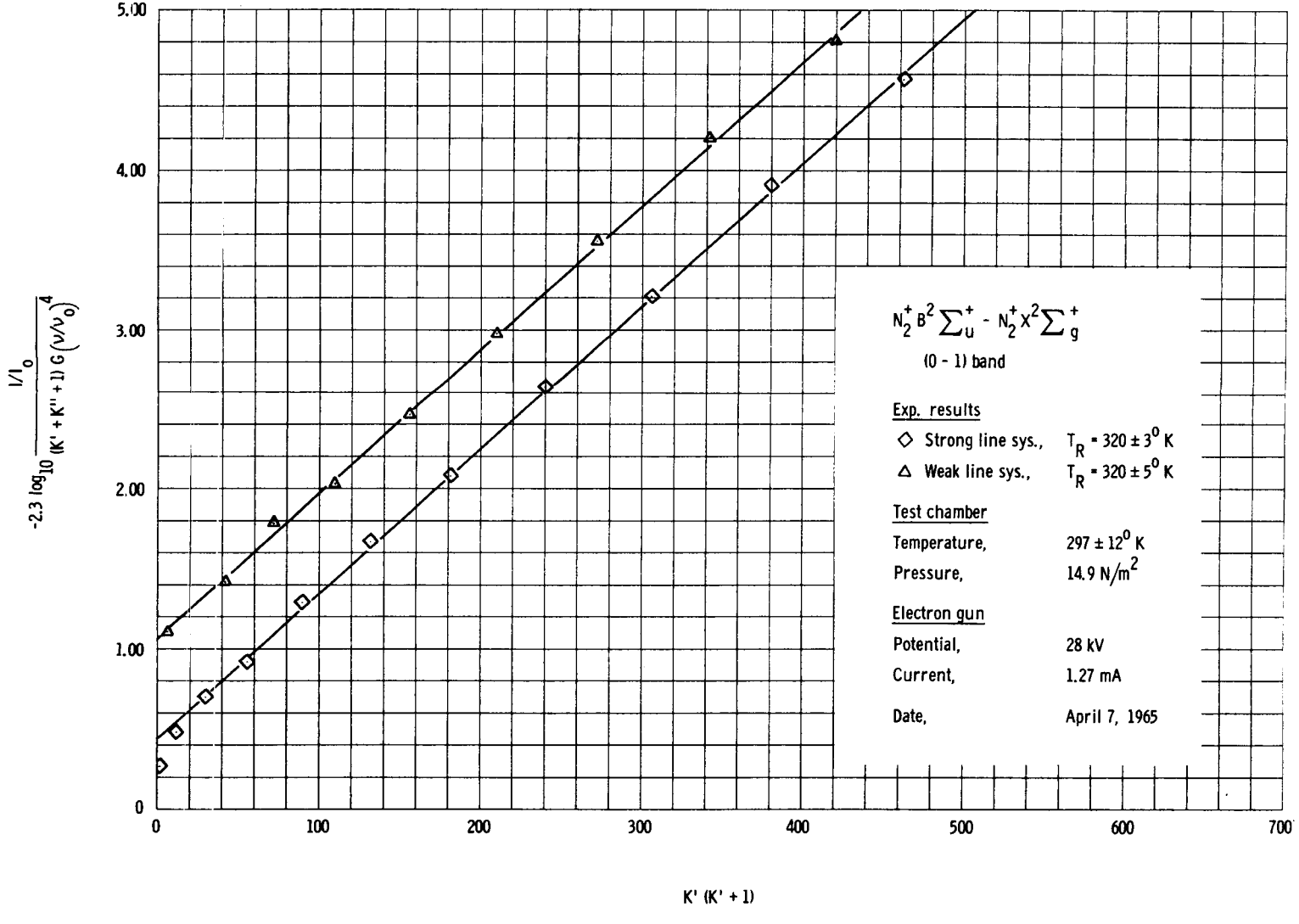

Figure 17.- 0-1 band data for 300° K experiment for T_R measurements.

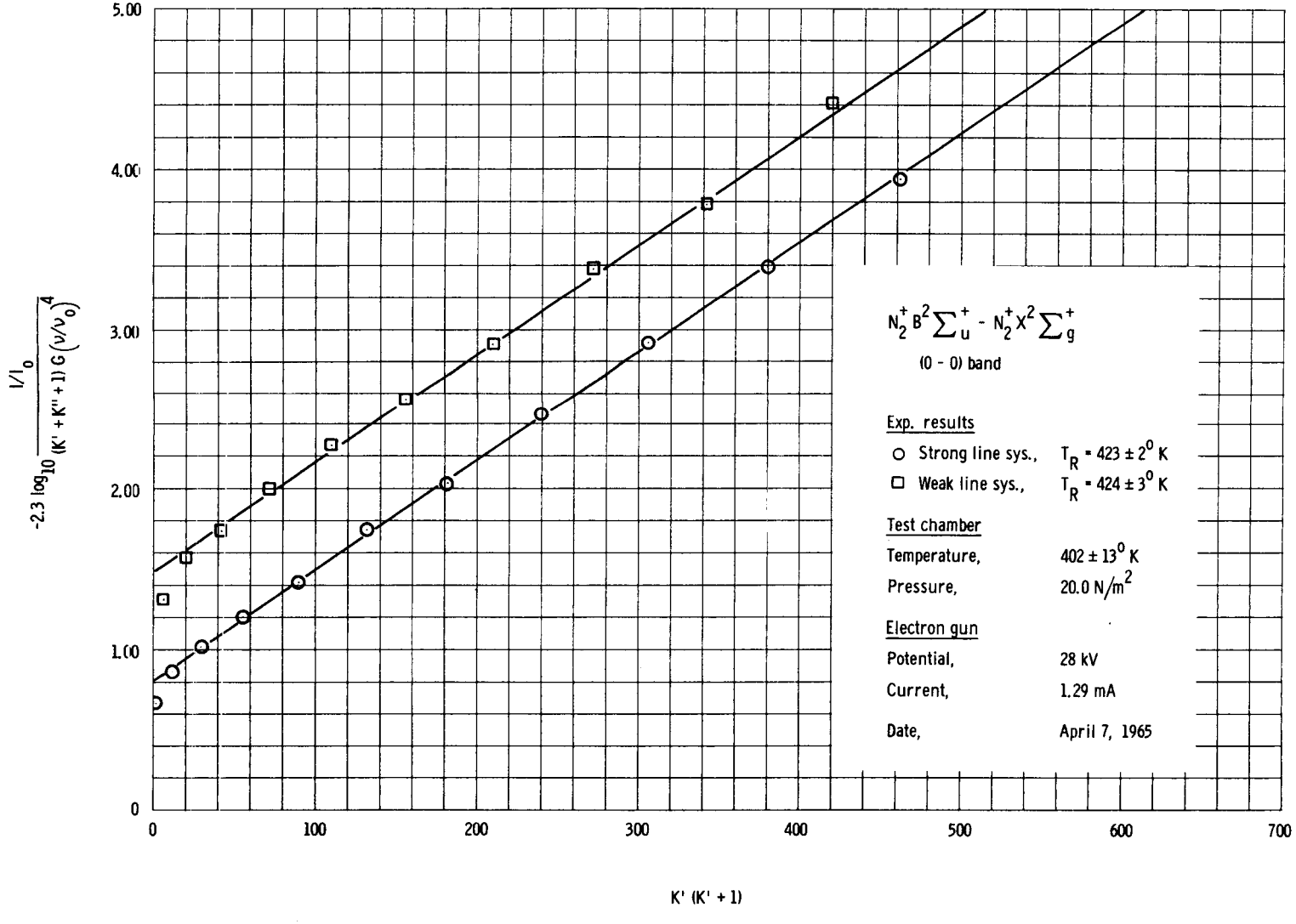

Figure 18.- 0-0 band data for 400° K experiment for T_R measurements.

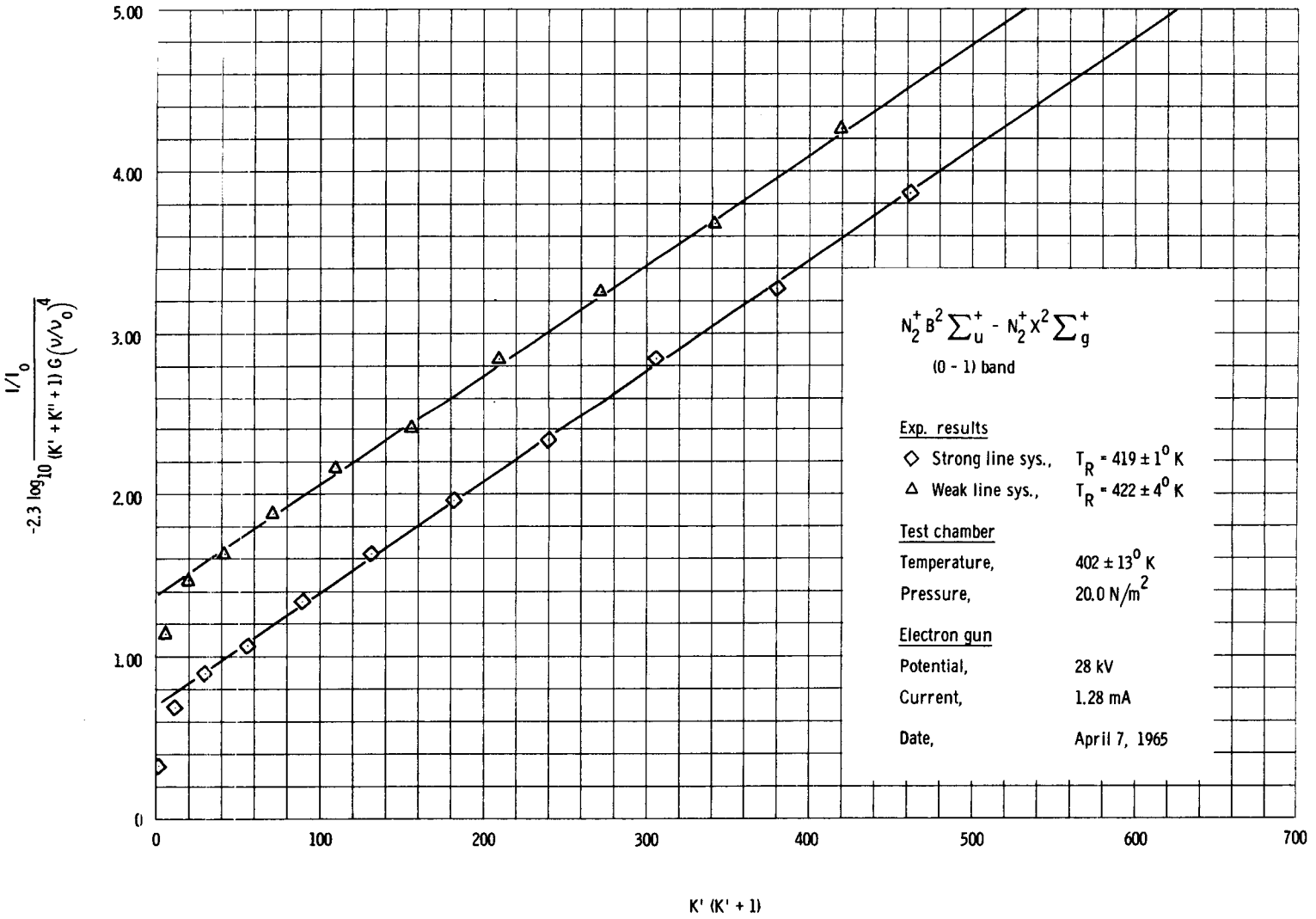

Figure 19.- 0-1 band data for 400° K experiment for T_R measurements.

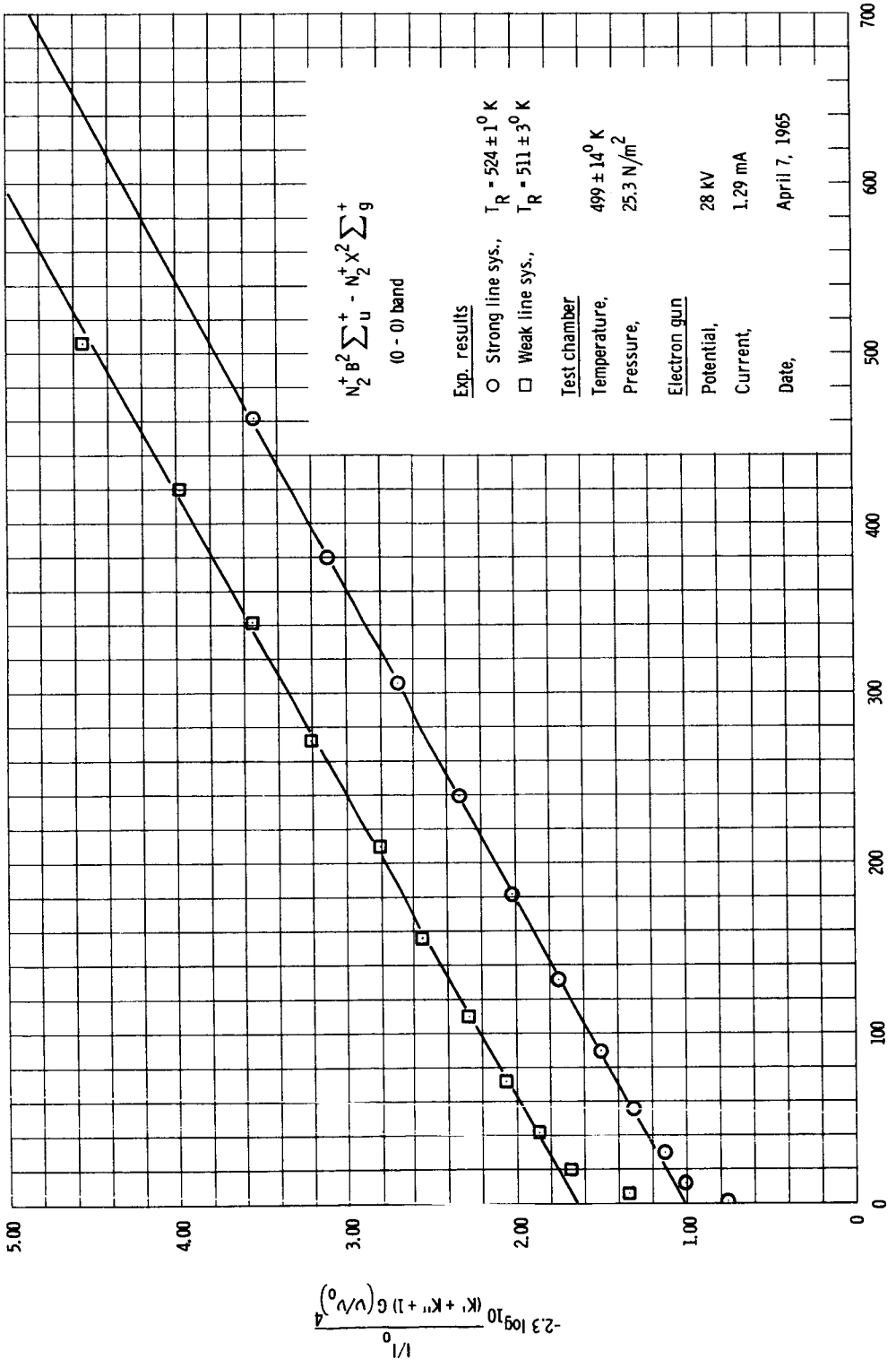

Figure 20.- 0-0 band data for 500° K experiment for T_R measurements.

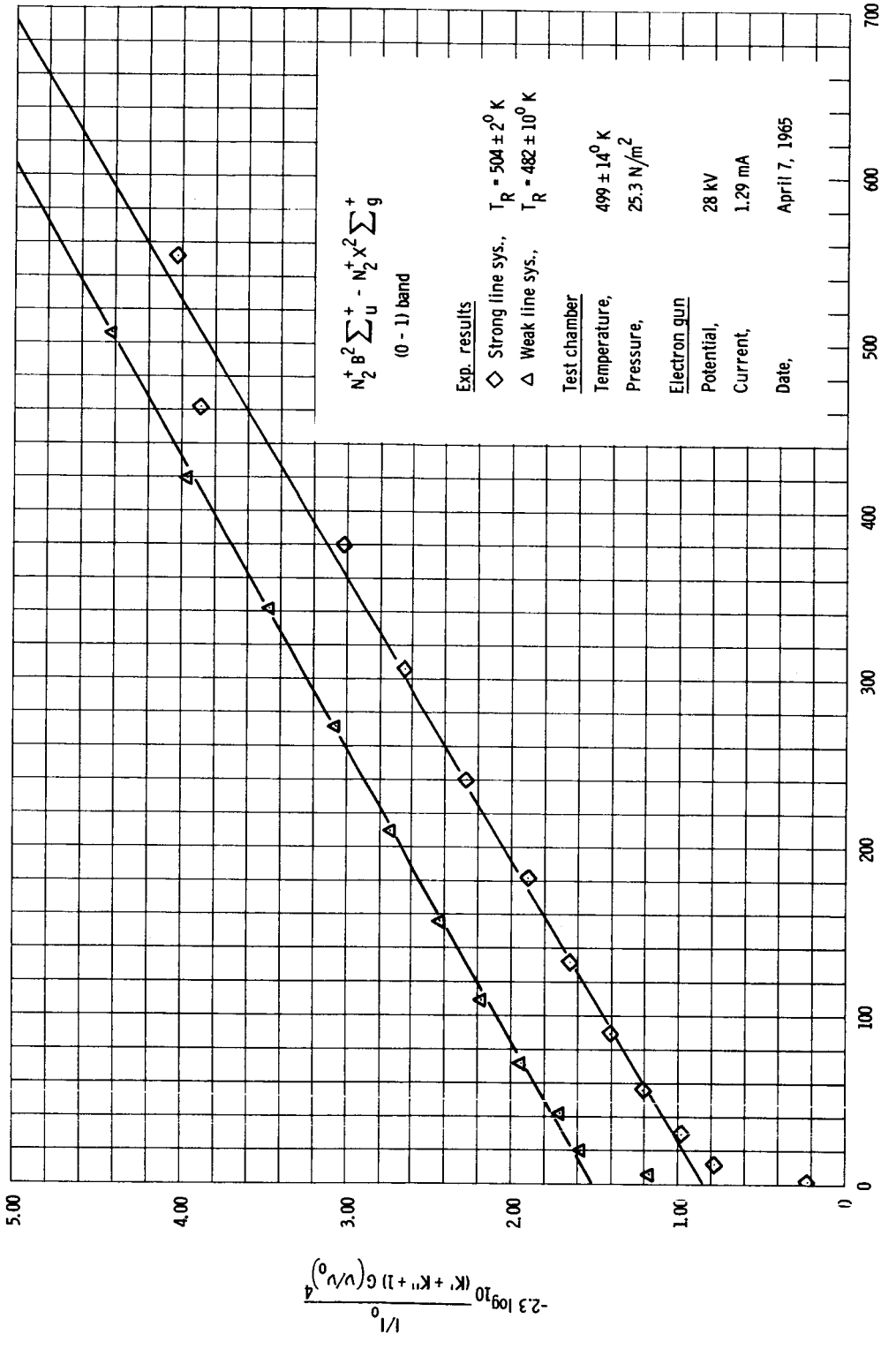

Figure 21.- 0-1 band data for 500° K experiment for T_R measurements.

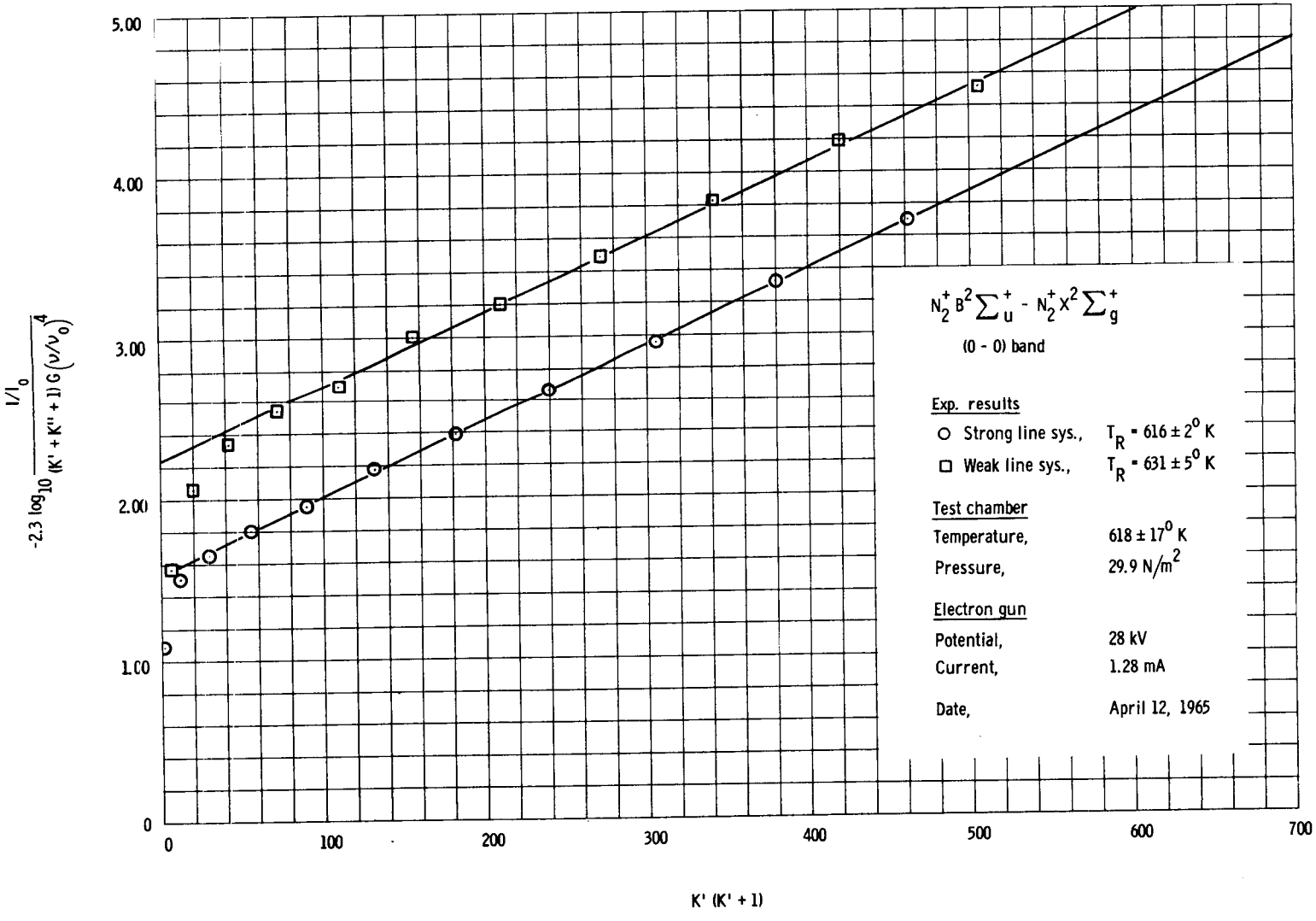

Figure 22.- 0-0 band data for 600° K experiment for T_R measurements.

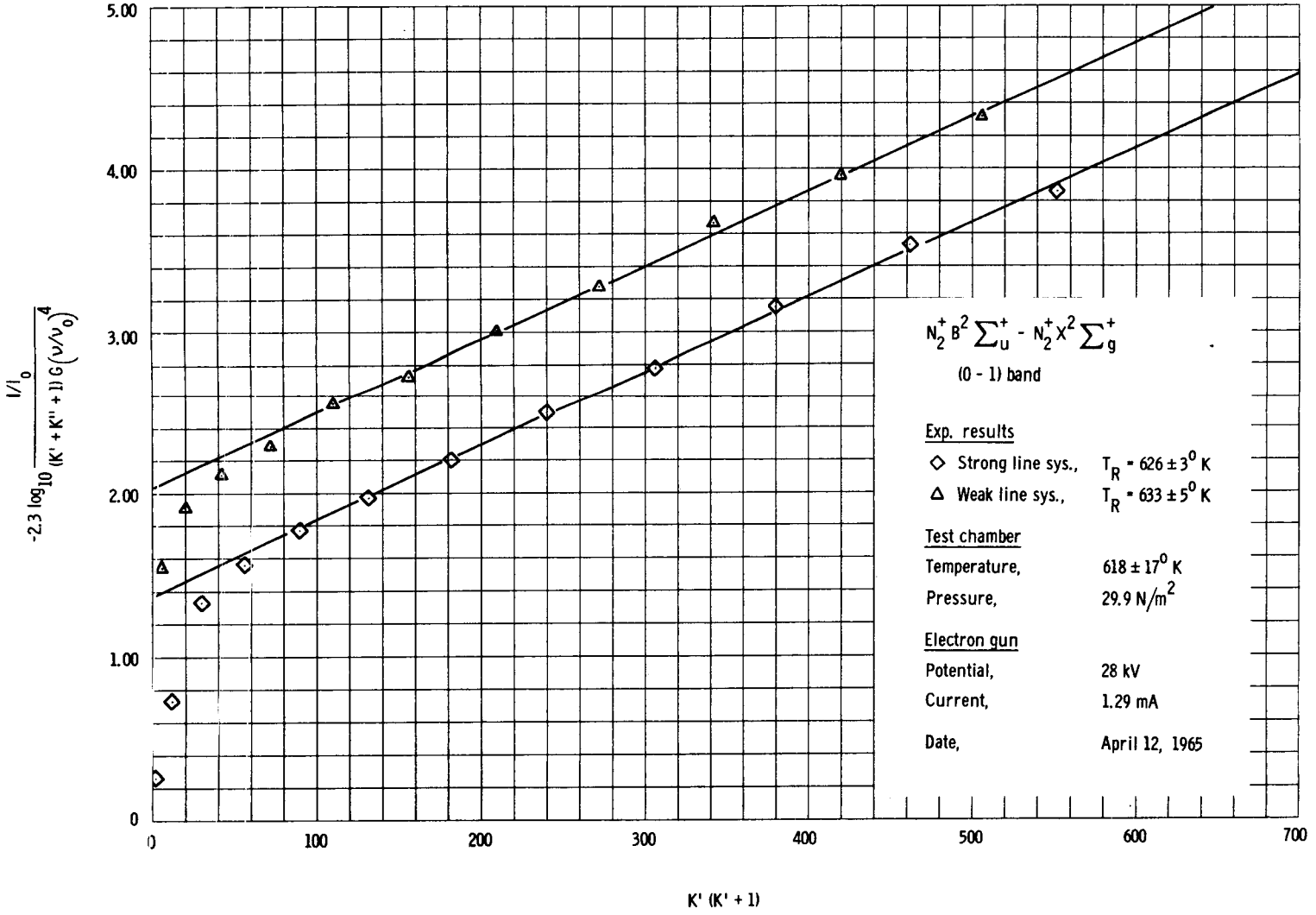

Figure 23.- 0-1 band data for 600° K experiment for T_R measurements.

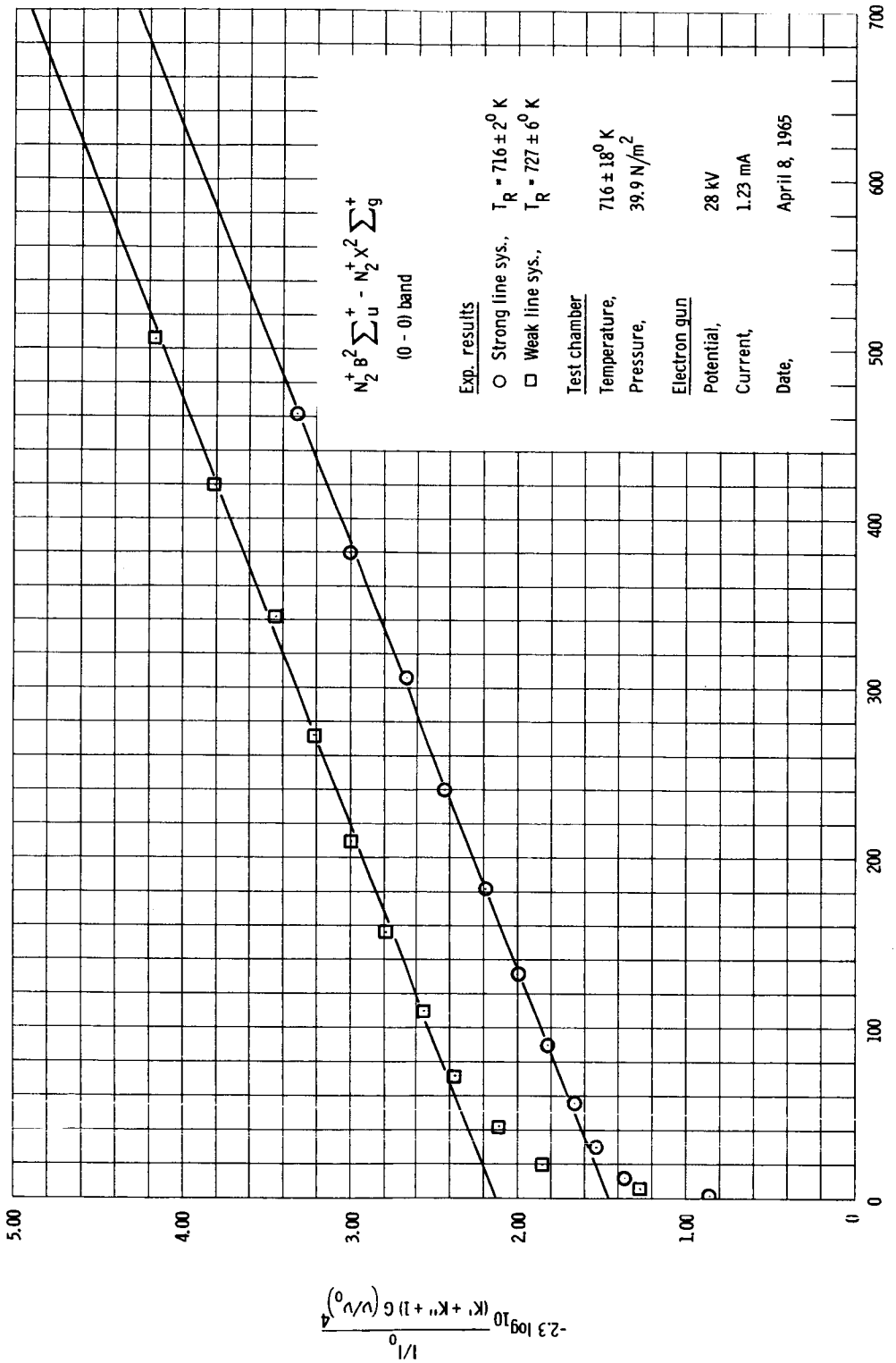

Figure 24.- 0-0 band data for 700° K experiment for T_R measurements.

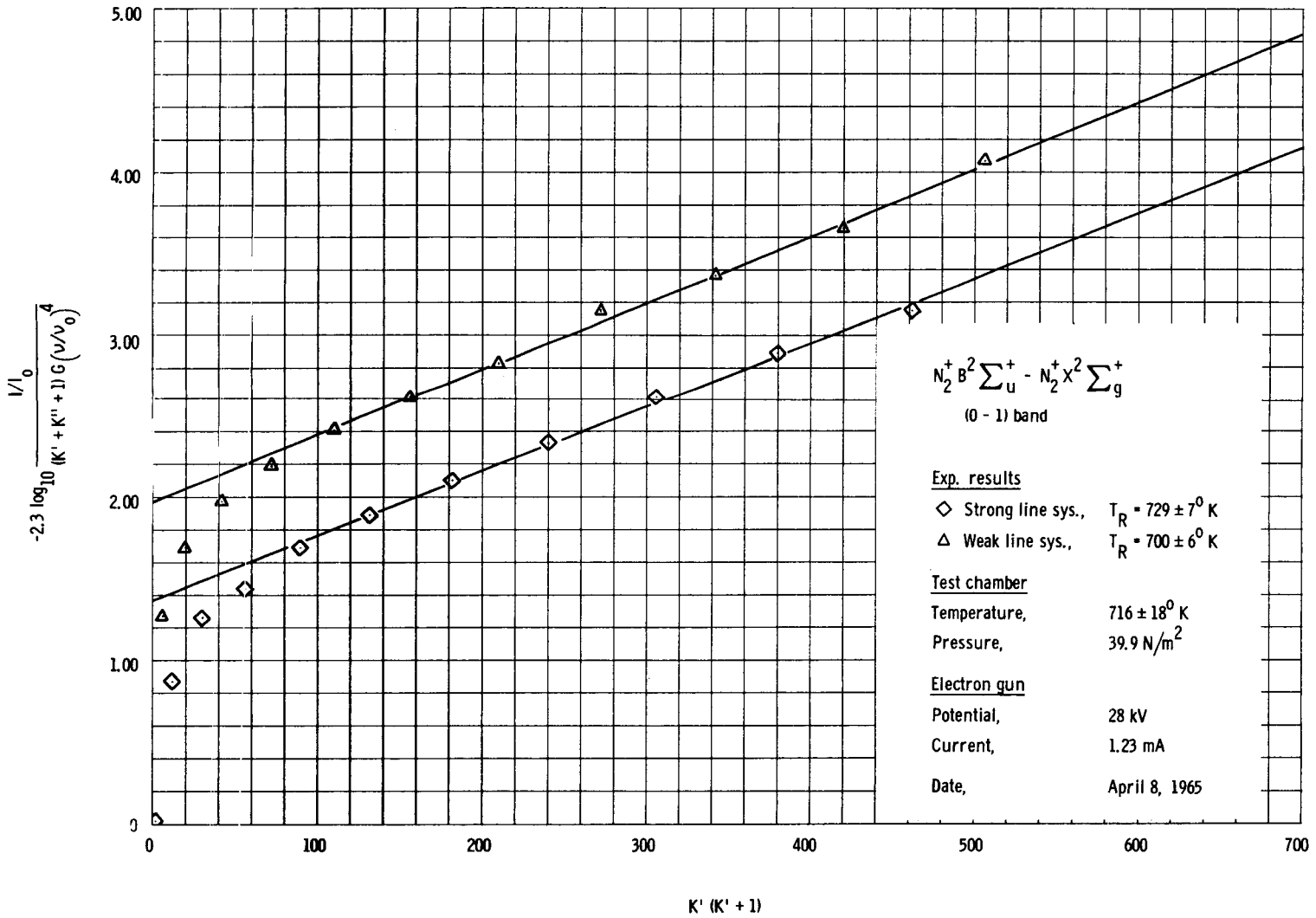

Figure 25.- 0-1 band data for 700° K experiment for T_R measurements.

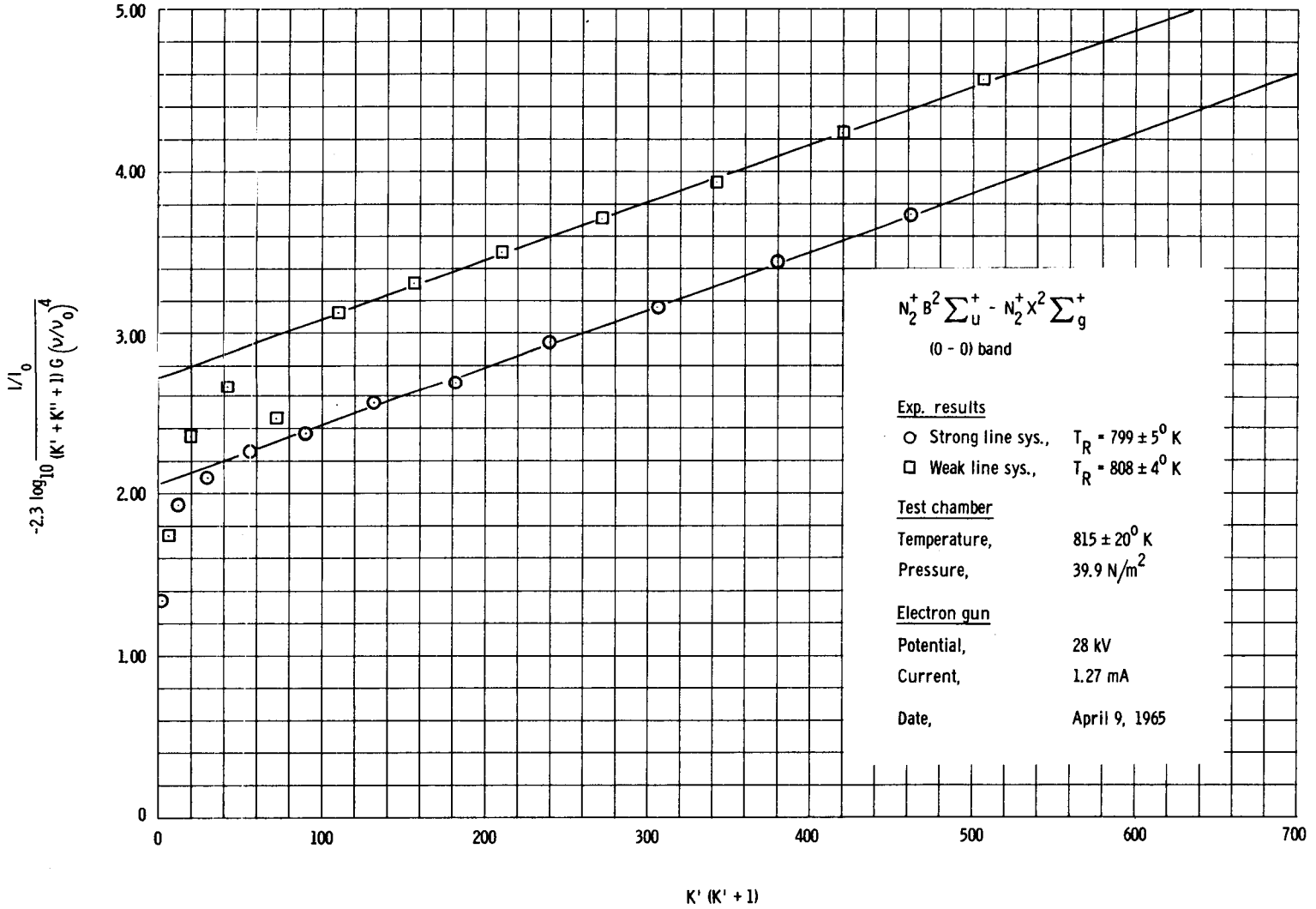

Figure 26.- 0-0 band data for 800° K experiment for T_R measurements.

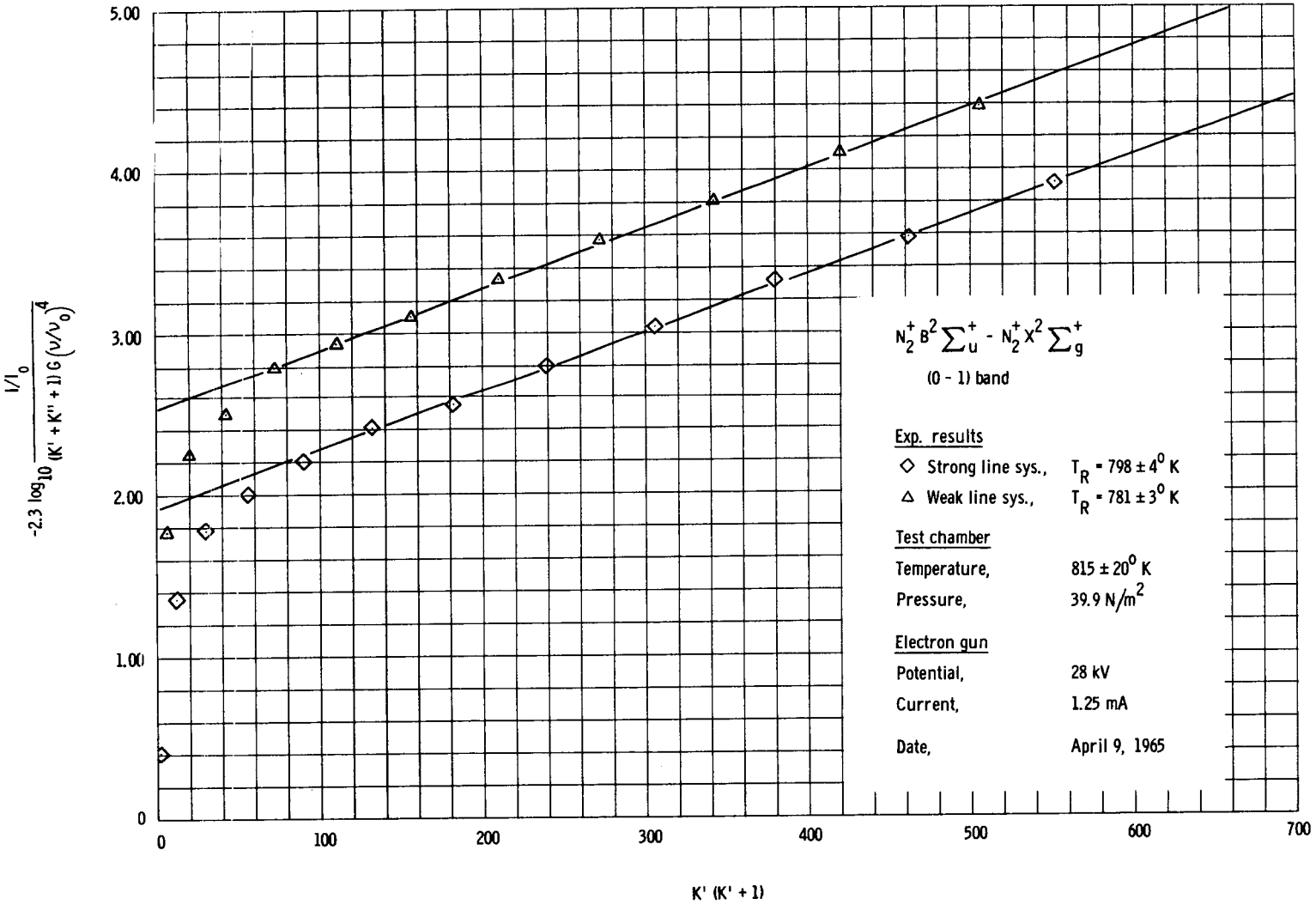

Figure 27.- 0-1 band data for 800° K experiment for T_R measurements.

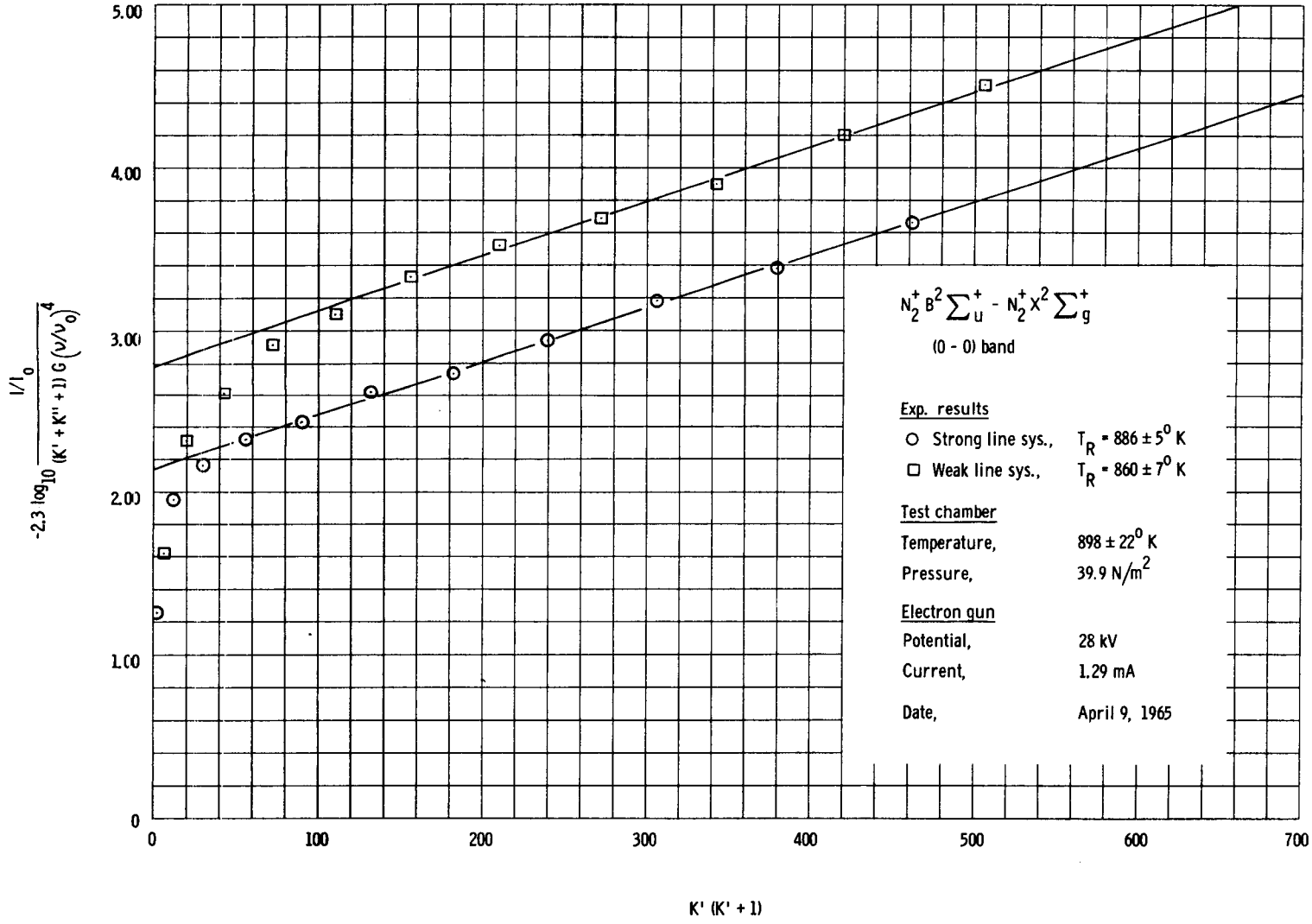

Figure 28.- 0-0 band data for 900° K experiment for T_R measurements.

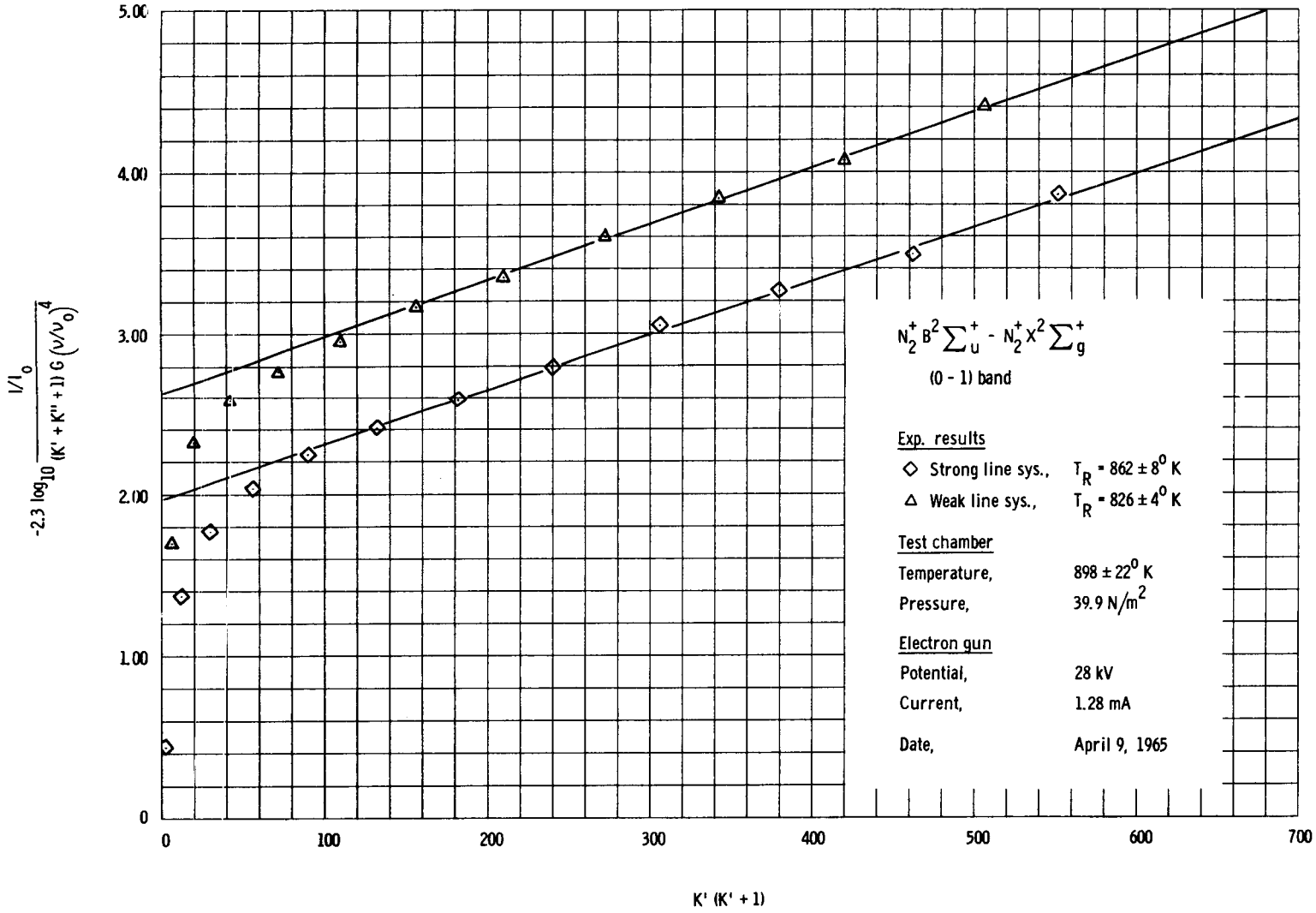

Figure 29.- 0-1 band data for 900° K experiment for T_R measurements.

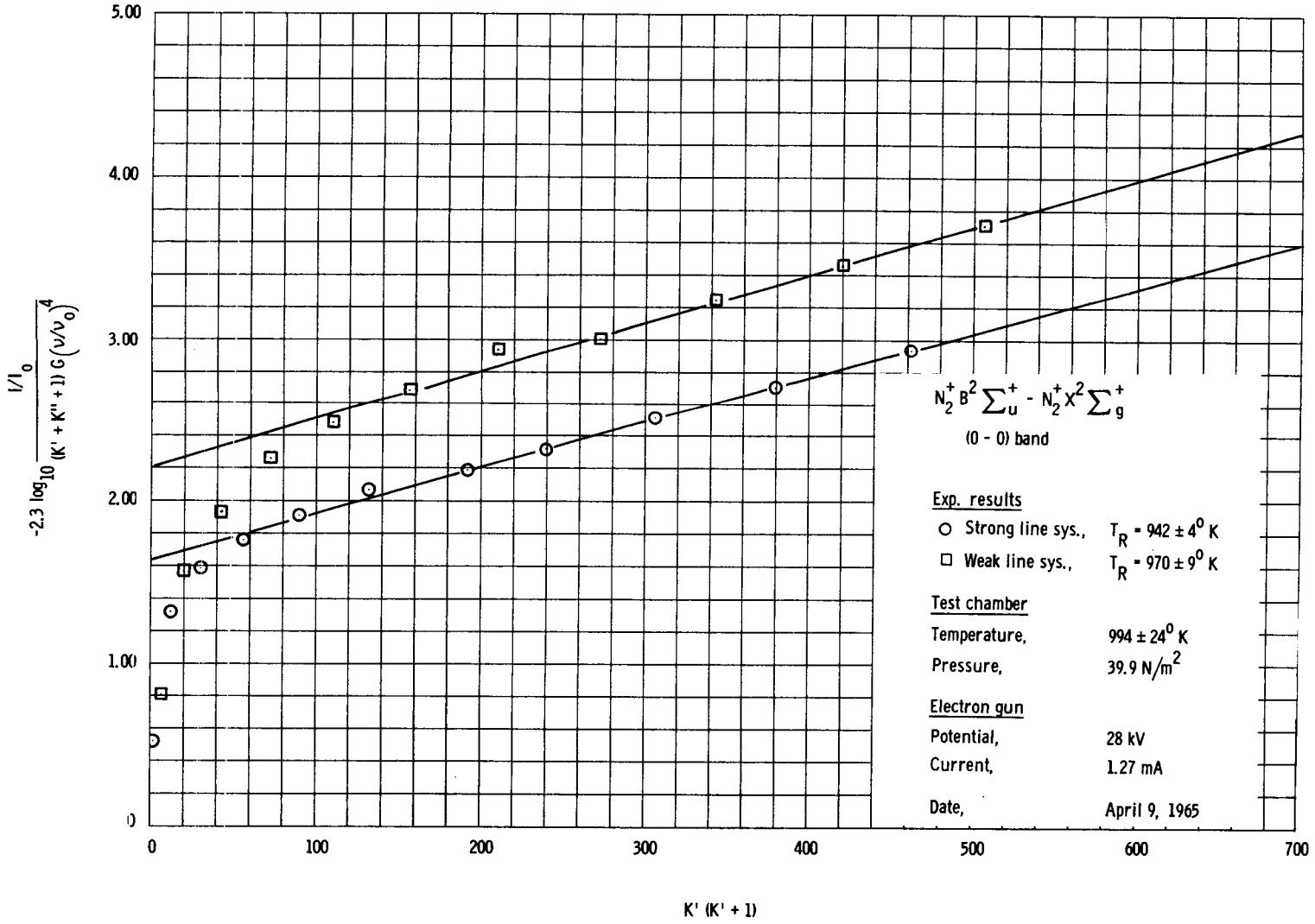

Figure 30.- 0-0 band data for 1000° K experiment for T_R measurements.

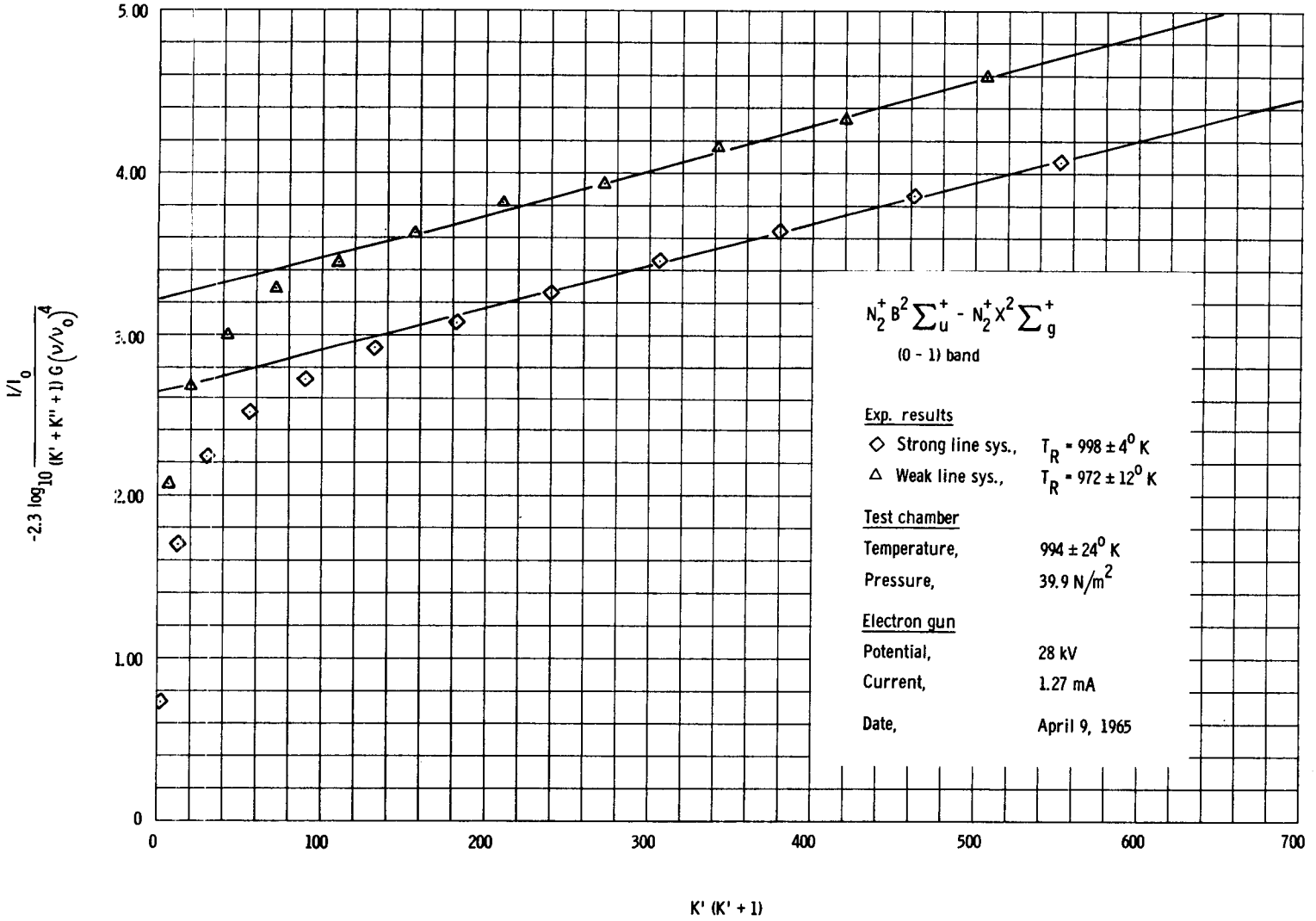

Figure 31.- 0-1 band data for 1000° K experiment for T_R measurements.

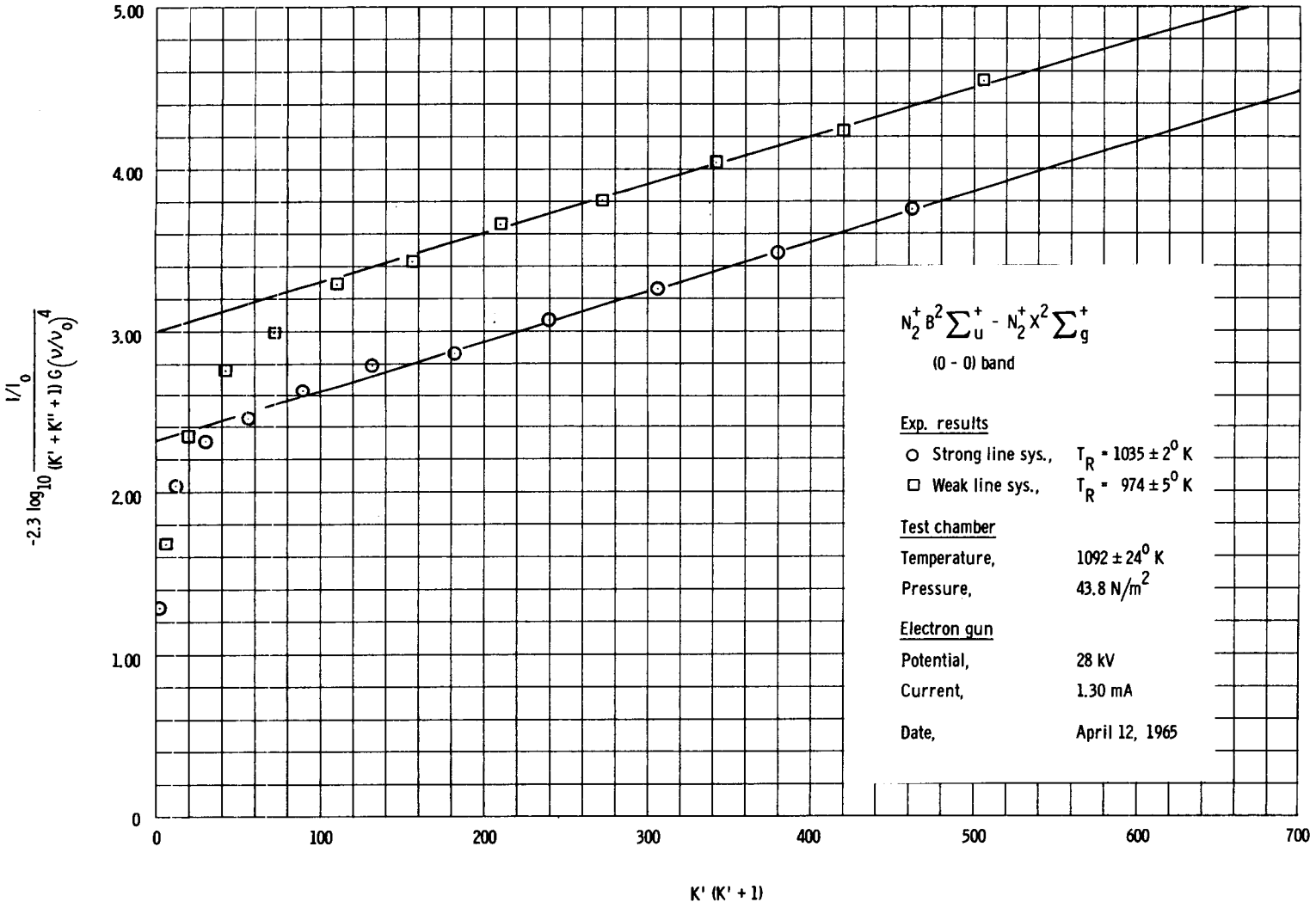

Figure 32.- 0-0 band data for 1100° K experiment for T_R measurements.

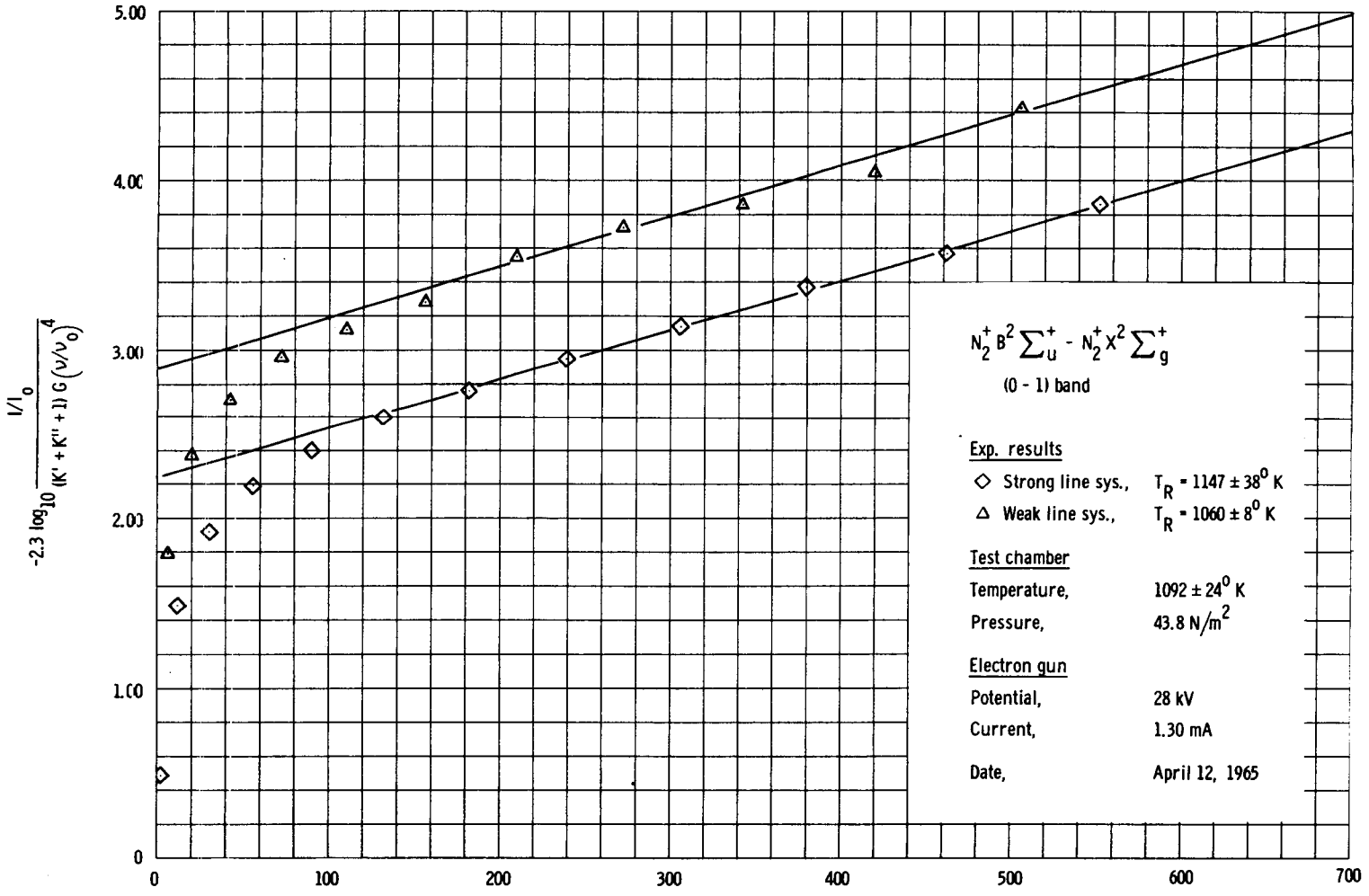

Figure 33.- 0-1 band data for 1100° K experiment for T_R measurements.

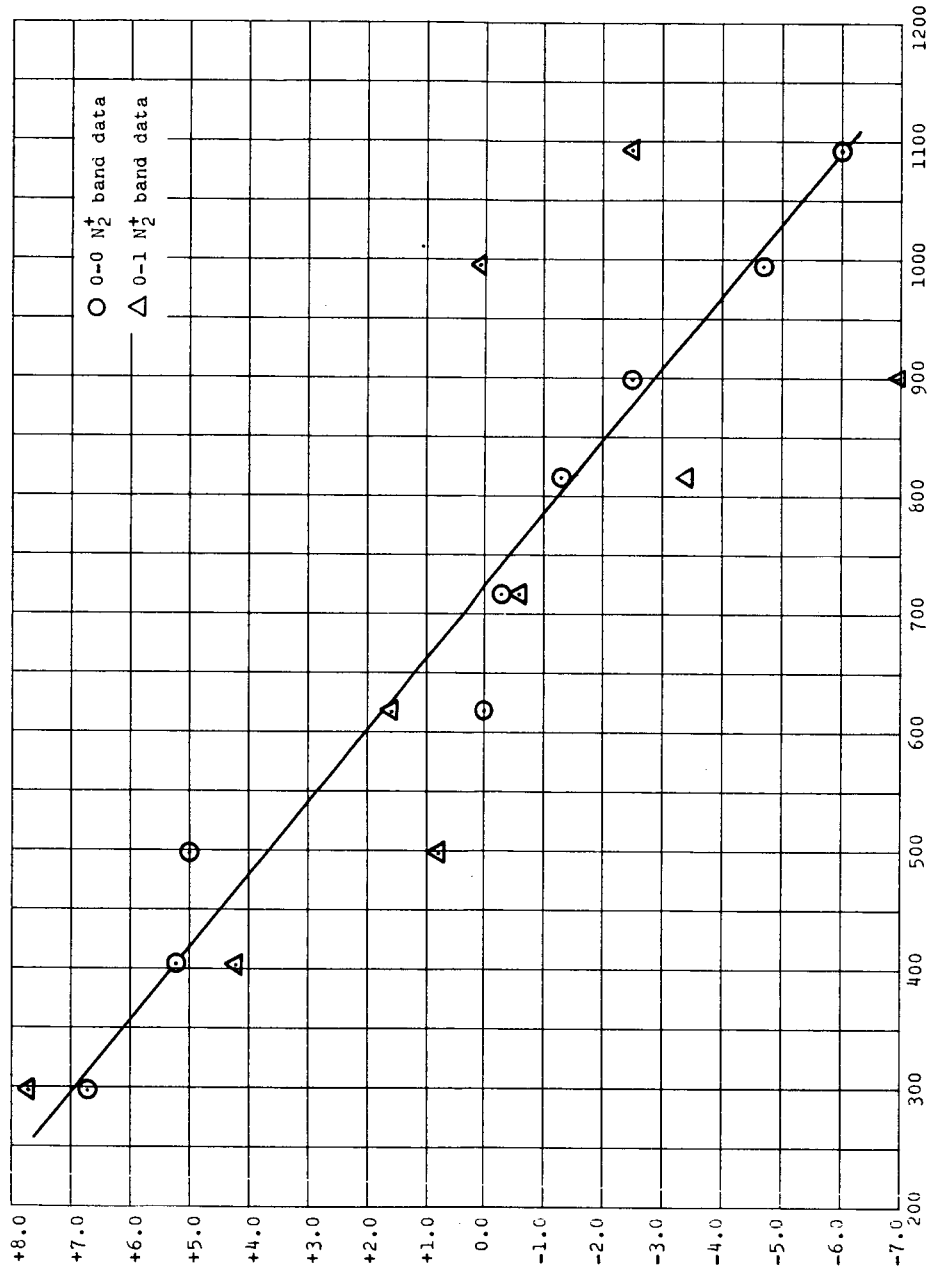

Figure 34.- Graph of percent difference between weighted mean T_R of 0-0 and 0-1 bands and reference temperature versus reference temperature.